PNAS PLUS

Defective synaptic connectivity and axonal neuropathology in a human iPSC-based model of familial Parkinson's disease

Georgia Kouroupi[a], Era Taoufik[a], Ioannis S. Vlachos[b], Konstantinos Tsioras[a], Nasia Antoniou[a], Florentia Papastefanaki[a], Dafni Chroni-Tzartou[a,c], Wolfgang Wrasidlo[d], Delphine Bohl[e,1], Dimitris Stellas[f], Panagiotis K. Politis[g], Kostas Vekrellis[h], Dimitra Papadimitriou[i], Leonidas Stefanis[h,j], Piotr Bregestovski[k], Artemis G. Hatzigeorgiou[b], Eliezer Masliah[d], and Rebecca Matsas[a,2]

[a]Department of Neurobiology, Hellenic Pasteur Institute, 11521 Athens, Greece; [b]DIANA-Lab, Hellenic Pasteur Institute, 11521 Athens, Greece; [c]Department of Neurology, Aeginition Hospital, University of Athens Medical School, 11528 Athens, Greece; [d]Department of Neurosciences, University of California, San Diego, La Jolla, CA 92093; [e]Institut Pasteur, 75015 Paris, France; [f]Department of Cancer Biology, Biomedical Research Foundation of the Academy of Athens, 11527 Athens, Greece; [g]Center for Basic Research, Biomedical Research Foundation of the Academy of Athens, 11527 Athens, Greece; [h]Center of Clinical Research, Experimental Surgery and Translational Research, Biomedical Research Foundation of the Academy of Athens, 11527 Athens, Greece; [i]Neurology Clinic, Henry Dunant Hospital Center, 11526 Athens, Greece; [j]Second Department of Neurology, University of Athens Medical School, 11527 Athens, Greece; and [k]Aix-Marseille Université, INSERM, Institut de Neurosciences des Systèmes, 13005 Marseille, France

Edited by Solomon H. Snyder, Johns Hopkins University School of Medicine, Baltimore, MD, and approved March 24, 2017 (received for review October 18, 2016)

α-Synuclein (αSyn) is the major gene linked to sporadic Parkinson's disease (PD), whereas the G209A (p.A53T) αSyn mutation causes a familial form of PD characterized by early onset and a generally severe phenotype, including nonmotor manifestations. Here we generated de novo induced pluripotent stem cells (iPSCs) from patients harboring the p.A53T mutation and developed a robust model that captures PD pathogenic processes under basal conditions. iPSC-derived mutant neurons displayed novel disease-relevant phenotypes, including protein aggregation, compromised neuritic outgrowth, and contorted or fragmented axons with swollen varicosities containing αSyn and Tau. The identified neuropathological features closely resembled those in brains of p.A53T patients. Small molecules targeting αSyn reverted the degenerative phenotype under both basal and induced stress conditions, indicating a treatment strategy for PD and other synucleinopathies. Furthermore, mutant neurons showed disrupted synaptic connectivity and widespread transcriptional alterations in genes involved in synaptic signaling, a number of which have been previously linked to mental disorders, raising intriguing implications for potentially converging disease mechanisms.

α-synuclein | axonal degeneration | dystrophic neurites | Parkinson's disease | small molecules

Parkinson's disease (PD) is the second most common neurodegenerative disease characterized by progressive loss of striatal-projecting dopaminergic neurons of the substantia nigra, resulting in debilitating motor deficits (1). Although motor symptoms are the obvious outward sign, the disease involves a more widespread neuronal dysfunction, leading to early and late nonmotor features such as hyposmia, depression, sleep disturbance, cognitive decline, and dementia (2, 3). The hallmark of PD pathology is the presence of neuronal inclusions, known as Lewy bodies or Lewy neurites, composed mainly of αSyn (4). These protein aggregates are found in various central nervous system areas, shifting the focus from a defect in dopamine neurons to a more widespread disruption that forms a basis for the nonmotor manifestations of PD (5).

Evidence from genetic, biochemical, and biophysical studies supports that αSyn monomers, oligomers (6), fibrils, and other conformers have central roles in the pathogenesis of PD and other synucleinopathies (7). αSyn is the major sporadic PD-linked gene (8), whereas point mutations (9) and multiplications (10) of the locus cause an autosomal dominant form of PD. The best-characterized mutation is p.A53T (G209A SNCA), first identified in families of Italian and Greek ancestry (11). A large number of p.A53T-based in vitro and in vivo animal models have been created for understanding the mechanisms of PD pathogenesis and progression and for assisting in drug development. However, an important limitation is the extent to which these experimental models recapitulate key neuropathological features of the human disease (12). Recent advances in cell-reprogramming technologies have allowed generation of induced pluripotent stem cells (iPSCs) from somatic cells of patients with sporadic or familial PD (13–19), offering the opportunity to elucidate disease phenotypes, investigate the underlying mechanisms, and screen for new drugs. However, it has been difficult to identify

Significance

Parkinson's disease (PD) is an incurable neurodegenerative disorder characterized by motor and nonmotor deficits, including cognitive decline and dementia. The protein αSyn is strongly associated with PD pathogenesis, whereas αSyn mutations, such as p.A53T, cause familial forms of PD. Animal models are crucial for understanding PD pathogenesis, but there are limitations in the extent to which these models reproduce faithfully the human disease. Cell-reprogramming technologies allow the generation of human neurons from patients with PD, but it has proven difficult to identify cellular pathologies in induced pluripotent stem cell–derived neurons. In this study, we created a robust p.A53T patient–derived model of PD that captures disease-related phenotypes under basal conditions, thus providing a unique system for studies of disease mechanisms and development of therapeutics.

Author contributions: G.K., E.T., and R.M. designed research; G.K., E.T., I.S.V., K.T., N.A., F.P., D.C.-T., D.S., P.K.P., and P.B. performed research; D.B. oversaw iPSC generation; A.G.H. supervised the bioinformatics analysis; W.W. and E.M. provided small-molecule inhibitors of αSyn aggregation; K.V., D.P., and L.S. provided patient fibroblasts; G.K., W.W., K.V., D.P., L.S., and E.M. contributed new reagents/analytic tools; G.K., E.T., I.S.V., N.A., F.P., P.B., A.G.H., and R.M. analyzed data; and G.K., E.T., and R.M. wrote the paper.

The authors declare no conflict of interest.

This article is a PNAS Direct Submission.

Data deposition: RNA-seq data have been deposited in Gene Expression Omnibus (accession no. GSE84684).

[1]Present address: Institut du Cerveau et de la Moelle épinière, INSERM U 1127, CNRS UMR-7225, Université Pierre et Marie Curie, Hôpital de la Pitié-Salpêtrière, 75013 Paris, France.

[2]To whom correspondence should be addressed. Email: rmatsa@pasteur.gr.

This article contains supporting information online at www.pnas.org/lookup/suppl/doi:10.1073/pnas.1617259114/-/DCSupplemental.

cellular pathologies in iPSC-derived PD neurons in the absence of oxidative or other cellular stress.

Here we generated de novo iPSC lines from two male patients with early disease onset who harbored the p.A53T αSyn mutation. By directed differentiation, we created a robust model containing dopaminergic, GABAergic, and glutamatergic neurons that displays disease-relevant phenotypes at basal conditions, including protein aggregation, compromised neurite outgrowth, and axonal neuropathology. Small molecules targeting αSyn reverted the degenerative phenotype under both basal and induced stress conditions, indicating that this strategy may be beneficial in individuals with PD and related disorders. Importantly, mutant neurons showed defective synaptic connectivity and remarkably dysregulated expression of genes involved in synaptic signaling, a number of which have been previously linked to schizophrenia, autism, and bipolar disorder. Our findings uncover disease-associated phenotypes, provide an unexpected link between PD and mental disorders that raises intriguing implications for potentially converging pathological mechanisms in psychiatric and neurologic diseases, and highlight a promising therapeutic strategy for PD and other synucleinopathies.

Results

Generation of iPSCs. Skin fibroblasts from two p.A53T patients (*SI Appendix*, Table S1 *A* and *B*, for clinical case description) and from one unaffected individual (control) were reprogrammed to iPSCs (20). All generated iPSC lines showed human embryonic stem cell (HUES)-like morphology and expressed pluripotency markers (*SI Appendix*, Fig. S1*A*). Two clones from each individual were analyzed further. The differentiation capacity of iPSCs was confirmed by in vitro (*SI Appendix*, Fig. S1*B*) and in vivo (*SI Appendix*, Fig. S1*C*) germ-layer differentiation assays. Global gene-expression profiling (*SI Appendix*, Fig. S1*D*) and RT-PCR for selected pluripotency markers (*SI Appendix*, Fig. S1*E*) demonstrated that iPSC clones were distinctly different from the originating fibroblasts and similar to HUES (21). The G209A SNCA mutation was detected in PD fibroblasts and PD-iPSCs but not in control cells (*SI Appendix*, Fig. S1*F*). Patient-derived and control iPSC clones exhibited normal karyotype throughout serial passaging (*SI Appendix*, Fig. S1*G*).

Neuronal Differentiation of iPSCs. PD and control iPSC lines were differentiated to dopaminergic neurons following a dual SMAD

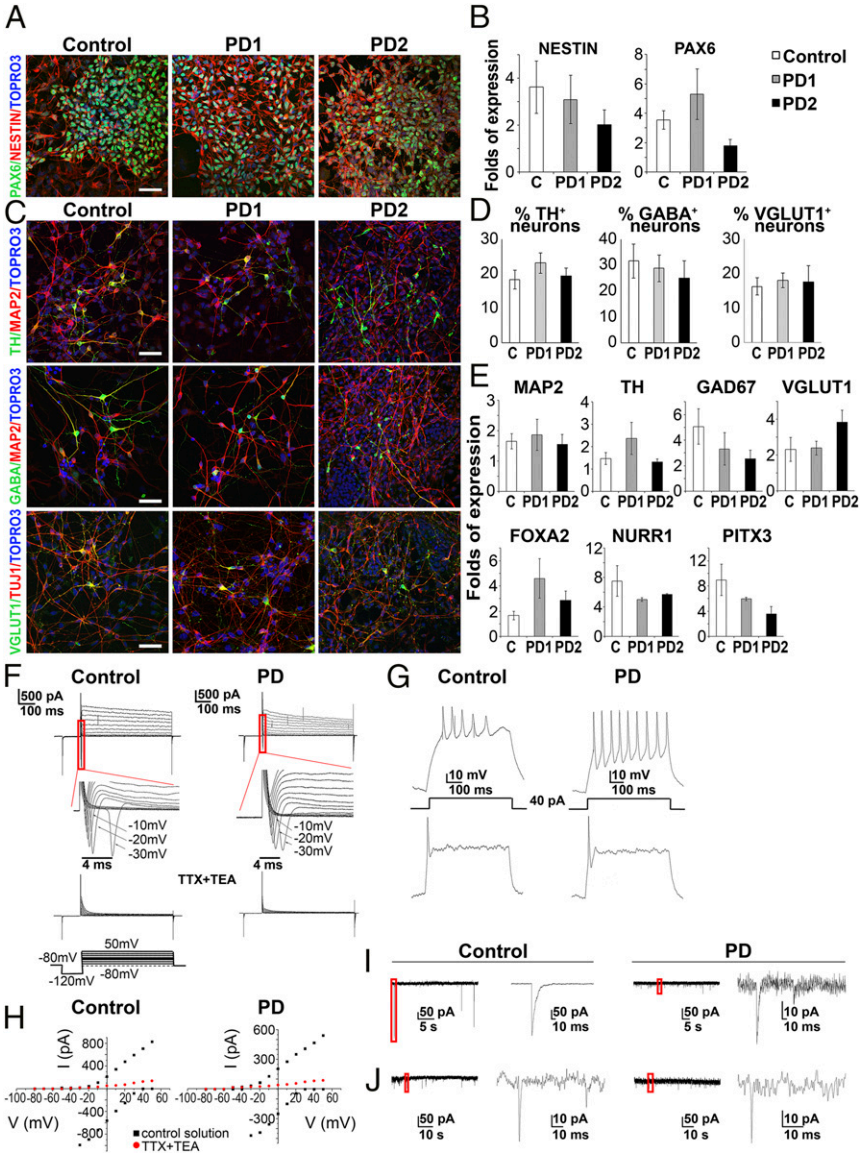

Fig. 1. Directed neuronal differentiation of iPSCs. (*A*) Immunostaining of control, PD1, and PD2 iPSC-derived NPCs for Pax6 (green) and Nestin (red). Cell nuclei are counterstained with TOPRO3 (blue). (Scale bar, 40 μm.) (*B*) RT-qPCR analysis of Nestin and Pax6 mRNA expression normalized to GAPDH levels. Data represent mean ± SEM (n = 3–5 for each cell line). (*C*) Immunostaining of iPSC-derived neurons at 50 DIV. Cells were stained (red) for MAP2 or βIII-tubulin (TUJ1) and (green) for TH (dopaminergic neuron marker), GABA (GABAergic neuron marker), and VGLUT1 (glutamatergic neuron marker). TOPRO3$^+$ nuclei are in blue. (Scale bar, 40 μm.) (*D*) Quantification of TH$^+$, GABA$^+$, and VGLUT1$^+$ neurons as percentage of MAP2$^+$ cells in control, PD1, and PD2 lines. Data represent mean ± SEM (n = 3–5 for each cell line). (*E*) RT-qPCR analysis of mRNA expression for MAP2, TH, GAD67 (GABAergic neuron marker), and VGLUT1, as well as for the dopaminergic lineage markers FOXA2, NURR1, and PITX3. Data represent mean ± SEM (n = 3–5 for each cell line). (*F–J*) Representative electrophysiological recordings from control and PD cells with typical neuronal morphology between 55 and 70 DIV. (*F*, *Upper* panels) Superimposed traces of currents evoked by depolarizing voltage steps (scheme of the protocol is shown in the *Bottom Left* panel). (*Insets* below *Upper* panels) Expanded from red lines rectangular traces of fast-activating, fast-inactivating inward Na^+ currents evoked by depolarizing voltage steps. (*Bottom* panels) Superimposed traces of currents evoked by the same set of depolarizing voltage steps after 1-min preapplication of TTX (tetrodotoxin, 1 μM) + TEA (tetraethylammonium, 20 mM). Note the strong inhibition of both inward and outward components. (*G*) Examples of voltage deflections and different patterns of action potential generation induced by current injections (40 pA). Current-clamp recordings from two control cells (*Left* traces) and two PD-derived cells (*Right* traces). Protocol of current step is shown. (*H*) Current–voltage relations of outward K^+ and inward Na^+ currents (black) under control conditions and after 1 min application of 1 μM TTX + 20 mM TEA (red). (*I* and *J*) Spontaneous synaptic activity of the neurons measured at −70 mV. GABAergic (*I*) and glutamatergic (*J*) synaptic currents are depicted.

inhibition protocol (22, 23) (*SI Appendix*, Fig. S2). Neural progenitor cells (NPCs) expressing Pax6 and Nestin were efficiently generated from control and PD iPSC lines (Fig. 1 *A* and *B*). Cells were further directed to differentiate into βIII-tubulin$^+$ and MAP2$^+$ neurons (Fig. 1*C*). At 50–60 days in vitro (DIV), 18–23% MAP2$^+$ neurons expressed tyrosine hydroxylase (TH; dopaminergic neurons: control—18.32 ± 2.7%; PD1—23.11 ± 2.9%; PD2—19.38 ± 2.3%; $n = 5$), 25–30% expressed the neurotransmitter GABA (GABAergic neuron marker: control—31.58 ± 6.5%; PD1—28.78 ± 5.2%; PD2—25 ± 6.6%; $n = 5$), and 16–18% expressed VGLUT1 (glutamatergic neuron marker: control—16.24 ± 2.4%; PD1—18.02 ± 2.1%; PD2—17.58 ± 4.7%; $n = 3$), as determined by immunofluorescence analysis (Fig. 1 *C* and *D*). RT-qPCR confirmed mRNA expression of the dopaminergic lineage markers FOXA2, NURR1, PITX3, and TH, as well as that of GAD67 and VGLUT1, respectively, characterizing GABAergic and glutamatergic neurons (Fig. 1*E*). In addition, next-generation transcriptome sequencing (RNA-seq) showed that both PD and control cultures expressed a number of immature and mature neuronal markers as well as neurotransmitter receptors (*SI Appendix*, Fig. S3*A*).

Functional maturation of iPSC-derived neurons was demonstrated by electrophysiology. Between 55 and 70 DIV, patch-clamp recordings showed that >70% of neurons exhibited transient inward sodium currents and sustained outward potassium currents (53 from 68 control cells and 52 from 64 PD cells) that could be blocked by specific pharmacological inhibitors (Fig. 1 *F* and *H*). Current-clamp recordings demonstrated that both control and PD cells developed the ability to fire action potentials in response to somatic current injections (Fig. 1*G*). Several output patterns were observed, including single bursts, repetitive firing, or trains of action potentials, indicating that iPSC-derived neurons had reached varying degrees of maturation. Additionally, cells responded to key neurotransmitters such as GABA, glutamate, glycine, and nicotine, confirming the presence of functional receptors (*SI Appendix*, Fig. S3*B*). Both PD and control neurons exhibited spontaneous synaptic activity, eliciting inhibitory (GABAergic) and excitatory (glutamatergic) postsynaptic currents (Fig. 1 *I* and *J*) that could be blocked by specific antagonists. Notably, expression of spontaneous synaptic activity was about twofold higher for control cells than for PD cells. Thus, in whole-cell recordings, 27.4% of control cells exhibited synaptic currents ($n = 62$), whereas only 16% ($n = 30$) and 12.5% ($n = 40$) of PD1 and PD2 cells, respectively, generated synaptic events.

Pathological Phenotypes in PD iPSC-Derived Neurons. PD-associated dementia is a major nonmotor manifestation, most prevalent in patients carrying the highly penetrant p.A53T mutation (24–26). Because p.A53T pathology is not limited to dopaminergic neurons, we took advantage of our iPSC-based system containing a mixed neuronal population as a more comprehensive model for p.A53T synucleinopathy.

Because the p.A53T mutation induces pathological αSyn aggregation (27), we confirmed by RNA-seq that the mutant SNCA allele is expressed in patient neurons (*SI Appendix*, Fig. S4). Immunofluorescence revealed that αSyn protein was present in the soma and neurites of both PD and control neurons, albeit more cells were strongly positive for αSyn in PD cultures (Fig. 2*A*). An increase in αSyn was confirmed in PD neurons by Western blotting, although quantification of αSyn mRNA by RT-qPCR did not show statistically significant differences between control and PD neurons (Fig. 2*C*). Notably, the pathological form of αSyn that is phosphorylated on serine 129 was detected primarily in PD cultures, revealing the existence of Lewy-like neurites by immunofluorescence (Fig. 2*B*), and in sister cultures by immunoblot (Fig. 2*C*).

Next, we examined potential aggregate formation by thioflavin S staining. Grain-like protein aggregates, also containing αSyn (*SI Appendix*, Fig. S5*A*), were detected in PD cultures at 50 DIV, whereas control neurons were completely devoid of thioflavin S-positive deposits (Fig. 2*D*). The protein nature of these aggregates was confirmed by treatment with proteinase K that efficiently cleared the majority of protein depositions in PD neurons (Fig. 2*D*). The presence of αSyn-positive protein aggregates inside inclusion bodies (aggresomes) was further validated using a fluorescence-based assay for detection of aggregated protein cargo (28) in combination with αSyn immunofluorescence (Fig. 2*D* and *SI Appendix*, Fig. S5*B*). Concomitant with aggregate formation, PD neurons started to exhibit distinct morphological features that distinguished them from control cells and were indicative of extensive neuritic pathology and degeneration. PD neuronal processes immunostained for βIII-tubulin (TUJ1) appeared more contorted with αSyn$^+$ swollen varicosities and large spheroid inclusions (Fig. 2 *E* and *F*) similar to the dystrophic neurites identified in the brain of p.A53T patients (29, 30). TUJ1$^+$/αSyn$^+$ swellings could be detected in otherwise morphologically intact axons, most likely marking an early event in neuritic degeneration (Fig. 2*F*, i). Quite often the distorted neurites of PD neurons ended up in fragmented processes reminiscent of the thread-like pathology found in the brain of p.A53T patients (29, 30) (Fig. 2*E*, arrow). Interestingly, the pathological phenotype of neuronal processes was not evident in cells stained for the somatodendritic marker MAP2, suggesting an axonal neuropathology, which was confirmed by staining for the axonal protein Tau (Fig. 2*G*; for quantification of axonal degeneration index, see Fig. 6*I*).

Taken together, these data show that an iPSC-based model of p.A53T PD recapitulates closely the neuropathological features identified in the brain of patients carrying the mutation, simulating reliably the human disease.

Synaptic Defects in PD iPSC-Derived Neurons. To gain molecular insight into the pathogenic mechanisms caused by the p.A53T mutation, we performed transcriptome-wide RNA-seq at specific stages of the differentiation procedure, corresponding to iPSCs, iPSC-derived NPCs (13 DIV) and neurons (48 DIV). Total RNA from two control lines (C1-1 and C1-2) and two PD lines (PD1-1 and PD1-2), the originating fibroblasts and from HUES, HUES-derived NPCs, and neurons, were used for cDNA library preparation. Following poly-A selection, RNA-seq was performed for global gene-expression profiling. Principal component analysis confirmed a reset in gene expression following fibroblast reprogramming and demonstrated that control and PD1 cells clustered primarily according to their differentiation stage, illustrating similar transcription profiles depending on cell state (Fig. 3 *A* and *B*). Nevertheless, a large number of differentially expressed mRNAs were identified between PD1 and control samples ($P < 0.05$; Fig. 3*C* and *SI Appendix*, Table S1*C*). In particular, 647 differentially expressed genes (379 down-regulated and 268 up-regulated) were identified between PD1-1/PD1-2 and C1-1/C1-2 neurons ($P < 0.05$; Fig. 3*D*). Of these, 34.62% ($n = 224$) corresponded to noncoding transcripts, including long noncoding RNAs ($n = 93$), antisense transcripts ($n = 37$), and pseudogenes ($n = 94$), and were excluded from further analysis.

Detailed bioinformatics analyses revealed several striking features of differentially expressed genes. Enrichment analysis based on Gene Ontology (GO), Kyoto Encyclopedia of Genes and Genomes (KEGG), and Reactome demonstrated significant perturbations in genes associated with metabolic function, cell cycle, extracellular matrix (ECM) and cytoskeletal organization, neuronal differentiation, maturation, and function (Fig. 3*E* and *SI Appendix*, Table S1*D*). Specifically, the alterations in GO categories of neurotransmitter receptor activity and binding, terminal button, nerve terminal, synapse, postsynaptic membrane, and ECM indicated that multiple neuronal pathways were compromised in PD neurons under basal culture conditions. Using Information Hyperlinked Over Proteins (iHOP) and PubMed–National Center

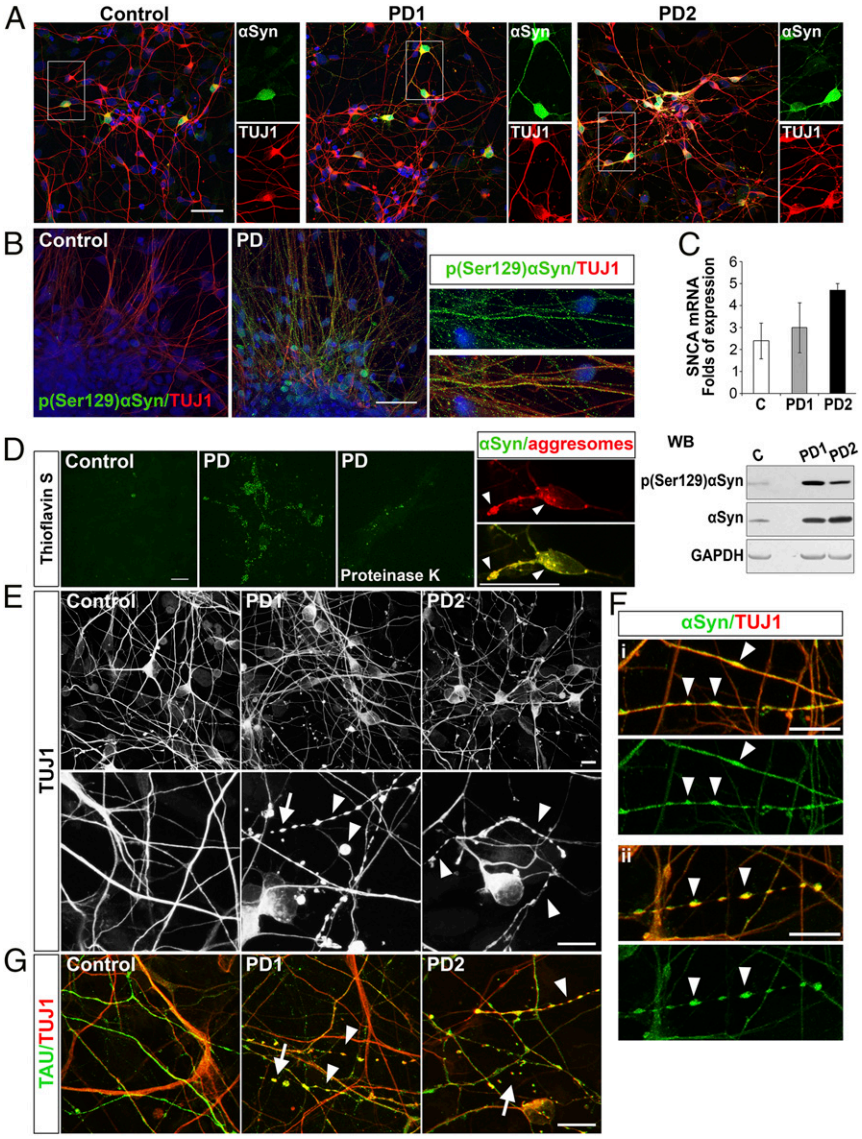

Fig. 2. Pathological phenotypes of PD iPSC-derived neurons. (*A*) Immunostaining for αSyn (green) and TUJ1 (red) in control, PD1, and PD2 iPSC-derived neurons at 50 DIV. (*Insets*) The marked regions at higher magnification. (Scale bar, 40 μm.) (*B*) Immunostaining for Ser129-phosphorylated αSyn [p(Ser129)αSyn] (green) and TUJ1 (red) in control and PD iPSC-derived neurons at 50 DIV. (Scale bar, 40 μm.) pS129 staining in PD neurites is shown at higher magnification (*Right*). (*C*, *Upper* graph) Quantification of αSyn mRNA by RT-qPCR in control (C), PD1, and PD2 iPSC-derived neurons at 48 DIV. Data represent mean ± SEM (n = 3–5 for each cell line). (*Lower* panel) Detection of αSyn and p(Ser129)αSyn by Western blot (WB); GAPDH shows equal protein loading. (*D*) Thioflavin S staining shows protein aggregates in PD cultures at 50 DIV. Clearance of protein depositions by proteinase K. (Scale bar, 20 μm.) Costaining of aggregated proteins (aggresomes; arrowheads; *Upper* micrograph in red) and αSyn (green) inside inclusion bodies (merged picture, *Lower* micrograph). (Scale bar, 20 μm.) (*E*) Immunostaining for TUJ1 in control, PD1, and PD2 iPSC-derived neurons at 50 DIV. Higher magnification (*Lower* panels) shows neurites with swollen varicosities and spheroid inclusions (arrowheads in PD1 and PD2 neurons) that frequently end up in fragmented processes (arrow). (Scale bar, 10 μm.) (*F*) Coimmunostaining for αSyn (green) and TUJ1 (red) in PD iPSC-derived neurons shows αSyn^{+} swollen varicosities (arrowheads) in neurites with earlier (i) and more advanced (ii) signs of degeneration. (Scale bars, 10 μm.) (*G*) Coimmunostaining for TUJ1 (red) and the axonal protein TAU (green) in iPSC-derived neurons reveals colocalization of the two proteins in swollen varicosities and axonal fragments. Arrowheads and arrows indicate blebbed and fragmented axons, respectively. (Scale bar, 10 μm.)

for Biotechnology Information, we identified 15 genes associated with PD and another nine with other related neurodegenerative diseases, such as Alzheimer's and Huntington's (*SI Appendix*, Table S1*E*). Importantly, a significant portion of altered mRNA transcripts (29 genes) was associated with psychiatric diseases, such as autism, schizophrenia, and bipolar disorder (*SI Appendix*, Table S1*E*), where synaptic dysfunction and eventually synaptic loss comprise the most prominent features (31–33). This was a rather unexpected finding that prompted us to further analyze gene transcripts encoding proteins involved in presynaptic vesicle formation and trafficking, vesicular and plasma membrane neurotransmitter transporters, axonal guidance, postsynaptic organization, and synaptic cell adhesion. In total, 92 relevant genes were altered; 80 were significantly down-regulated and 12 were up-regulated (*SI Appendix*, Table S1 *F*–*K*). Of those, 20 encoded for presynaptic proteins (*SI Appendix*, Table S1*F*), 18 for postsynaptic molecules (*SI Appendix*, Table S1*G*), 18 for trans-synaptic adhesion molecules (*SI Appendix*, Table S1 *H* and *I*), and 14 for axon guidance proteins (*SI Appendix*, Table S1*J* and Fig. 4 *A*–*E*). Selected genes representative of the above categories were validated by RT-qPCR using independent samples of PD1-1, PD1-2, C1-1, and C1-2, as well as two clones of the second patient (PD2-1 and PD2-2). For all 16 genes tested, significant down-regulation was confirmed in both clones from PD1 and PD2 (Fig. 4*G*). Of these, SYN3, SV2C, RPH3A, and DOC2B are found in the presynaptic area, where they are involved in synaptogenesis and neurite extension, synaptic vesicle organization, spontaneous synaptic vesicle exocytosis, and regulation of neurotransmitter release, respectively (34–37). Three of six members of the human SLITRK family (SLITRK1, -2, and -4) located at the postsynaptic membrane to act as organizers of excitatory synapse formation (38) were also down-regulated in PD1 and PD2 neurons, with SLITRK2 and -4 being hardly detectable. DLGAP2, another synaptic organizer enriched in the postsynaptic density (PSD) (39), as well as GRIN2D and GRIP2, which encode the NMDA glutamate receptor subunit ε-4 and the glutamate receptor interacting protein 2, respectively, were all down-regulated in PD1 and PD2 neurons. Two genes of the cadherin/proto-cadherin family (*SI Appendix*, Table S1*J*), CDH13 and CDH15 (40), were dramatically down-regulated in PD1 and PD2 neurons, further enhancing our notion of defective synapse formation and function.

Secreted glycoproteins belonging to the WNT family (41) are another class of molecules that promote synaptogenesis and regulate synaptic function. The mRNA expression of the family members WNT3A, WNT5A, WISP1, RSPO1, RSPO3, FRZB, and DKK2 was found differentially expressed (*SI Appendix*,

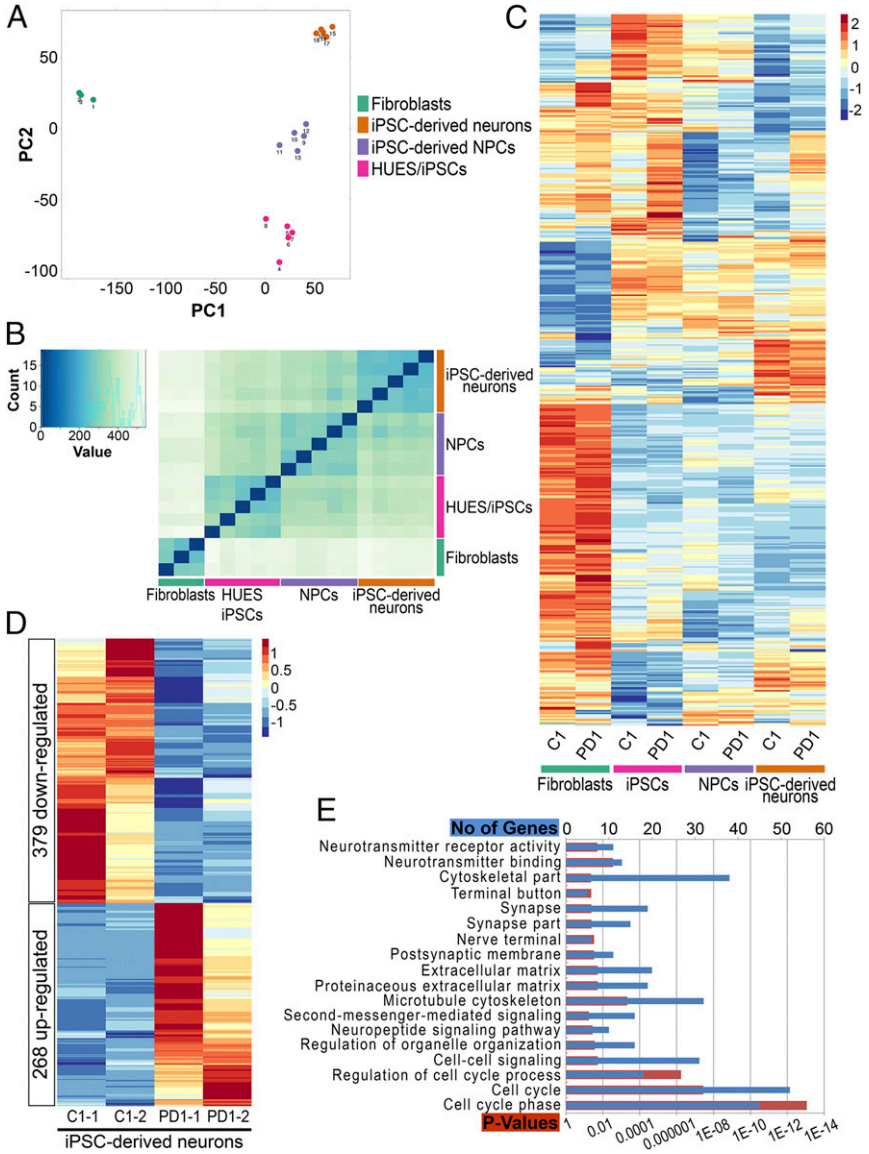

Fig. 3. Summary of RNA-seq analysis. (*A*) Graph depicting the first two principal components (PC1 and PC2) of all sequenced samples. Principal component analysis was performed on the 1,000 genes having the highest expression variance across all samples. All groups exhibit distinct expression patterns and within-group uniformity. Samples: fibroblasts (green)—1, fetal; 2, control (C1); and 3, PD1; HUES/iPSCs (magenta)—4, HUES; 5, C1-1 iPSCs; 6, C1-2 iPSCs; 7, PD1-1 iPSCs; and 8, PD1-2 iPSCs; iPSC-derived NPCs (purple)—9, HUES-NPCs; 10, C1-1 NPCs; 11, C1-2 NPCs; 12, PD1-1 NPCs; and 13, PD1-2 NPCs; iPSC-derived neurons (orange)—14, HUES-neurons; 15, C1-1 neurons; 16, C1-2 neurons; 17, PD1-1 neurons; and 18, PD1-2 neurons. (*B*) Sample gene expression distance heat map calculated using all expressed genes in all samples: fibroblasts (green), HUES/iPSCs (magenta), NPCs (purple), and iPSC-derived neurons (orange). (*C*) Heat map depicting the expression of the 500 genes with the highest mean expression across all sequenced samples. (*D*) Heat map of differentially expressed transcripts between PD1-1/PD1-2 and C1-1/C1-2 iPSC-derived neurons. A total of 647 differentially expressed transcripts (268 up-regulated and 379 down-regulated) were detected between PD and control neurons ($P < 0.05$). Higher expressions are in red, and lower expressions are in blue. (*E*) Enrichment analysis of the significantly ($P < 0.05$) altered genes in the RNA-seq analysis of PD versus control iPSC-derived neurons against GO terms.

Table S1*K*). Notably, a significant number of calcium-associated proteins (*SI Appendix*, Table S1*L*, and Fig. 4*F*), such as RCN3, HPCA, CCBE1, CACNA2D4, and CACNA1D, together with various neurotransmitter receptors and channels (*SI Appendix*, Table S1*G*) known to be involved in synaptic function and neurotransmission (42), were also significantly down-regulated at the mRNA level. Of these, RCN3, HPCA, GRI2ND, and GRIP2 were validated by RT-qPCR in both PD1 and PD2 neurons (Fig. 4*G*). Overall, our data show that the p.A53T mutation affects the expression of pre- and postsynaptic genes involved in different processes of synapse formation, maturation, and function. A number of genes associated with axon guidance were also perturbed in PD1 neurons (*SI Appendix*, Table S1*J* and Fig. 4*E*) with FABP7 and ABLIM3 verified in both PD1 and PD2 (Fig. 4*G*).

To investigate potential consequences of synaptic gene dysregulation, we assessed the ability of control and PD neurons to form synaptic connections. To this end, neurons were seeded on a feeder layer of mouse primary astrocytes to enhance their maturation for up to 100 DIV. In these cultures, the characteristic immunofluorescence puncta of the presynaptic protein synapsin1 (SYN1) were clearly detected on the neurites of control and PD neurons at 70 and 100 DIV (Fig. 5*A*). However, costaining of SYN1 with MAP2 revealed less complex neuronal networks with thinner or less fasciculated neuronal processes in PD neurons. Additionally, in many PD neurons, SYN1 was retained mainly in

the soma rather than in the processes (Fig. 5*A*). Synapse formation was identified by coimmunostaining for SYN1 and the postsynaptic marker PSD95 (Fig. 5*B*). Quantification of the number of $SYN1^+/PSD95^+$ puncta pairs showed a 27% reduction in the number of synaptic contacts in PD neurons at 70 DIV (control 2.64 ± 0.18 pairs per 10 μm vs. PD 1.93 ± 0.15 pairs per 10 μm, $P = 0.005$; Fig. 5*C*) and a 22% reduction at 100 DIV (control 2.86 ± 0.26 pairs per 10 μm vs. PD 2.22 ± 0.13 pairs per 10 μm, $P = 0.045$; Fig. 5*D*), a phenotype strongly linked to the dysregulated expression of synaptic genes identified in p.A53TαSyn neurons.

Rescue of Neuropathological Phenotypes of PD Neurons by Small Molecules Targeting αSyn. Because the molecular perturbations in PD neurons indicated dysregulation in neurostructural processes and network formation, we further examined the morphology of control and PD neurons 7 d after transduction with a lentiviral vector for expression of the red fluorescent protein DsRed under the control of the human synapsin 1 promoter (LV. SYN1.DsRed) to facilitate imaging of single neurons (Fig. 6*A*).

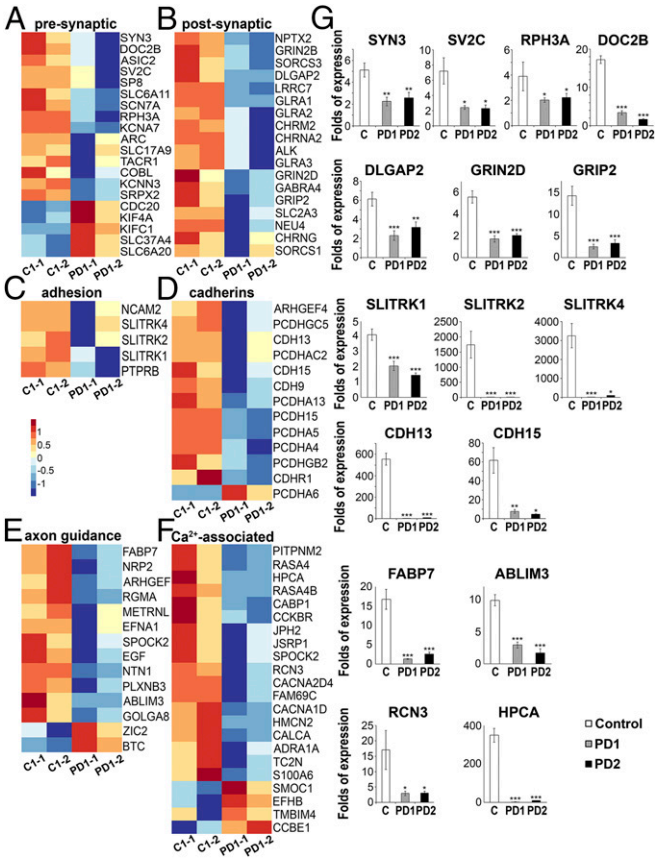

Fig. 4. Gene expression analysis of iPSC-derived neurons. (*A–F*) Differential gene expression between control (clones C1-1 and C1-2) and PD1 (clones PD1-1 and PD1-2) iPSC-derived neurons at 48 DIV. Heat maps of genes encoding presynaptic (*A*) and postsynaptic proteins (*B*), trans-synaptic adhesion molecules (*C*), cadherins (*D*), axon guidance molecules (*E*), and calcium-associated proteins (*F*). High expressions are in red and low expressions are in blue. (*G*) RT-qPCR analysis of selected genes in control (C), PD1, and PD2 iPSC-derived neurons at 48 DIV: presynaptic SYN3, SV2C, RPH3A, and DOC2B; postsynaptic DLGAP2 and receptors GRIN2D and GRIP2; trans-synaptic adhesion SLITRK1, -2, and -4; cadherins CDH 13 and 15, genes associated with axon guidance FABP7 and ABLIM3; and calcium-associated RCN3 and HPCA. Gene expression normalized to GAPDH. Data represent mean ± SEM (one-way ANOVA, $*P < 0.05$, $**P < 0.01$, $***P < 0.001$, $n = 3–5$ for each cell line).

Although at 50 DIV soma size was comparable (Fig. 6*B*), neurite length was significantly reduced in PD neurons (control: 293.91 ± 27.39 μm; PD1: 142.85 ± 19.80 μm; PD2: 102.45 ± 15.35 μm; control vs. PD1: $P < 0.0001$; control vs. PD2: $P < 0.0001$; Fig. 6*C*), as well as the total number of neurites extending from the soma (control: 3.97 ± 0.12; PD1: 3.42 ± 0.14; PD2: 3.15 ± 0.14; control vs. PD1: $P = 0.011$; control vs. PD2: $P < 0.0001$; Fig. 6 *D* and *E*). To check whether this phenotype is causally related to pathological p.A53T-αSyn, we used three de novo in silico-designed compounds—NPT100-18A (43), NPT100-14A (patent #8,450,481), and ELN484228 (44)—that all interact with and reduce αSyn toxicity by interfering with αSyn oligomer formation through distinct mechanisms. Their addition in the 1 to 20 nM range did not induce toxicity in control or PD neurons. All three compounds could quench the differences observed in neurite length between control and PD1 neurons when added at a final concentration of 2 nM throughout the neuronal differentiation period (Fig. 6*F*). Treatment with NPT100-18A that interacts with the C terminus of αSyn was most effective in restoring the number of neurites extending from the soma of PD neurons (DMSO: 3.72 ± 0.22; NPT100-18A: 4.83 ± 0.24; ELN484228: 4.23 ± 0.22; NPT100-14A: 3.8 ± 0.19; DMSO vs. NPT100-18A: $P = 0.013$; Fig. 6*G*), whereas it had no effect in control neurons (DMSO: 4.68 ± 0.23; NPT100-18A: 4.53 ± 0.26; ELN484228: 4.4 ± 0.28; NPT100-14A: 4.5 ± 0.34; Fig. 6*G*). Importantly, all three compounds rescued to a large extent the dramatic pathology observed in $TUJ1^+$ PD neurons as they alleviated significantly the existence of distorted/degenerating axons, with NPT100-18A and ELN484228 being most effective (axon degeneration index: control–DMSO: 1 ± 0.13; PD1–DMSO: 8.83 ± 0.67; PD1–NPT100-18A: 2.89 ± 0.29; PD1–ELN484228: 3.34 ± 0.31; PD1–NPT100-14A: 5.59 ± 1.21; control–DMSO vs. PD1–DMSO: $P < 0.0001$; PD1–DMSO vs. PD1–NPT100-18A: $P < 0.0001$; PD1–DMSO vs. PD1–ELN484228: $P < 0.0001$; PD1–DMSO vs. PD1–NPT100-14A: $P = 0.002$; Fig. 6 *H* and *I*). Overall, these observations causally link the disease-related phenotypes of PD neurons to αSyn pathology.

Reversal of Induced-Stress Phenotypes of PD Neurons by Small Molecules Targeting αSyn. To check whether the above-used small molecules were also effective under induced stress conditions, we accelerated neuronal degeneration and cell death by treatment with the proteasome inhibitors epoxomicin and MG-132 that interfere with αSyn clearance via the proteasome. Initial experiments confirmed a dose-dependent induction of cell death by both inhibitors as assessed by lactate dehydrogenase (LDH) release and an increased sensitivity of PD neurons to proteasome stress (*SI Appendix*, Fig. S6). In subsequent experiments, each inhibitor was added for 24 h at the concentration that induced the largest difference between control and PD cells. Epoxomicin (1 μM) and MG-132 (10 μM) treatment evoked a significant increase in cleaved caspase 3 immunoreactivity and a pronounced disruption of the $MAP2^+$ network (Fig. 7*A*), consistent with the levels of LDH release in PD neurons (Fig. 7 *B* and *C*). Quantification of LDH release also revealed that untreated PD neurons were more susceptible to death (Fig. 7 *B* and *C*).

We then performed a series of induced stress experiments in neurons treated with NPT100-18A, NPT100-14A, or ELN484228. At 48 DIV, neurons were replated, and 7–9 d later, epoxomicin and MG-132 were added for 24 h. Epoxomicin-treated PD neurons showed an extensively degenerate $MAP2^+$ network that was most effectively protected by NPT100-18A and to a lesser extent by NPT100-14A and ELN484228 (Fig. 7*D*). Similar results were obtained in MG-132–treated PD neurons, where NPT100-18A and NPT100-14A preserved the $MAP2^+$ network (Fig. 7*E*).

Discussion

We report pathological phenotypes and protective effects of small-molecule inhibitors of αSyn aggregation in iPSC-derived

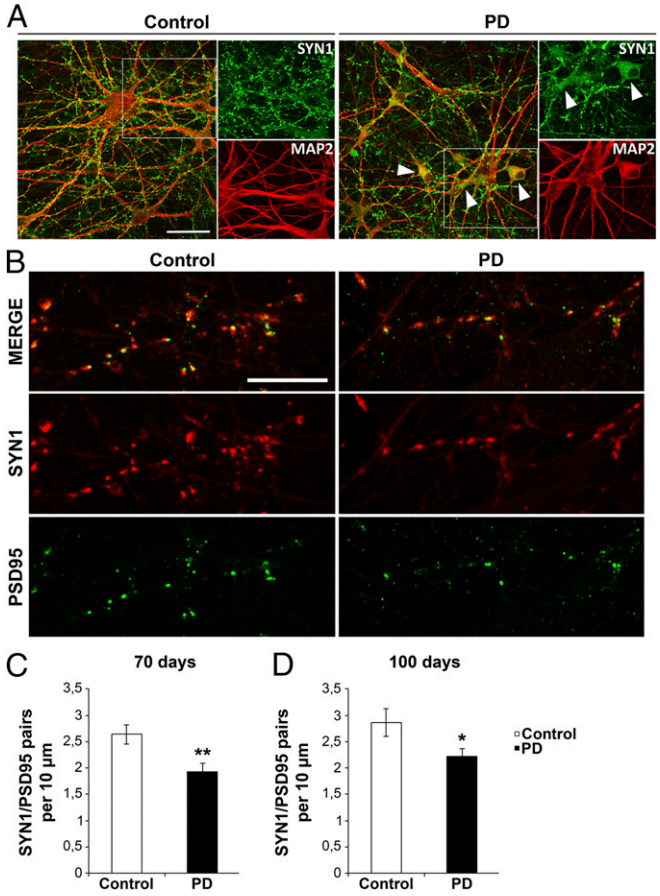

Fig. 5. Synaptic connections in iPSC-derived neurons. (*A*) Immunofluorescence puncta of the presynaptic protein synapsin 1 (SYN1, green) in control and PD MAP2-positive (red) neurons seeded on mouse astrocytes and maintained for 100 DIV. Arrowheads indicate that SYN1 remains in the soma of many PD neurons in contrast to control neurons. (*Insets*) The marked regions at higher magnification. (Scale bar, 40 µm.) (*B*) Maximum projection confocal images showing $SYN1^+$ (red) and $PSD95^+$ (green) synaptic puncta pairs in control and PD neurons. (Scale bar, 10 µm.) (*C* and *D*) Quantification of the number of $SYN1^+/PSD95^+$ puncta pairs per 10 µm at 70 DIV (*C*) and at 100 DIV (*D*) in control and PD neurons. Data represent mean ± SEM (Student's *t* test, $*P < 0.05$, $**P < 0.01$).

neurons from patients with PD carrying the p.A53T mutation. Our data strongly support an iPSC-based model that faithfully simulates disease pathogenesis and uncovers disease-relevant phenotypes under basal conditions. These include protein aggregation, compromised neuritic outgrowth, and axonal αSyn/Tau-associated pathology, resulting in decreased synaptic connectivity. Accordingly, mutant neurons showed a profound dysregulation in the expression of genes involved in synaptic signaling, including genes associated with synapse formation, trans-synaptic adhesion, and postsynaptic organization. Importantly, small molecules targeting αSyn could correct the degenerative phenotype of PD neurons, thus providing a direct mechanistic link and a therapeutic strategy that may be beneficial for patients with PD and related disorders.

In addition to its involvement in rare familial PD cases, αSyn consists of the major sporadic PD-linked gene identified so far, underlying its importance in PD initiation and progression. Patients harboring the p.A53T mutation in αSyn manifest prominent motor and nonmotor symptoms, including autonomic dysfunction, cognitive decline, dementia, and psychotic features (25, 26) (*SI Appendix*, Table S1*B*). It is now recognized that a stronger focus on the nonmotor symptoms is essential for assessing and treating the disease-specific and drug-induced psychiatric symptoms. Additionally, increasing evidence suggests that the neuropsychological deficits seen early in the course of the disease might also be a powerful predictor of the overall progression of cognitive dysfunction to dementia, with implications for early pharmacological intervention (45). Our findings from human iPSC-derived neurons suggest that disruption of synaptic connections may form a basis for the nonmotor deficits in p.A53T patients with PD.

A striking finding in our study is that patient-derived neurons capture PD neuropathological processes over a relatively short period in culture and in the absence of induced stress. They exhibit thioflavin S-positive aggregates, αSyn-containing intracellular inclusion bodies, and extensive neuritic pathology with grain-like inclusions and knotted spheroids, similar to the structures detected in the neocortex, deep cortical areas, hippocampus, forebrain, and midbrain of p.A53T patients (29, 30). Interestingly, the appearance of swellings marked an early event in neuritic degeneration. In agreement, overexpression of mutant p.A53T-αSyn in rats induced dystrophic axons and alterations in axonal transport that preceded neuronal loss (46). Tau-positive inclusions were also prominent, indicating a severe axonal pathology consistent with the presence of extensive Tau lesions in the brains of p.A53T patients (29). Our data support the hypothesis that Tau and αSyn are involved in shared or converging pathways in the pathogenesis of PD, as well as in the development of cognitive impairment and dementia in patients with familial and possibly also idiopathic PD (47, 48). These findings have important implications for understanding the interface between Tau and αSyn pathways in neurodegenerative disorders.

The extensive axonal pathology and the degenerative phenotype of PD neurons could be rescued by small-molecule inhibitors that interfere specifically with αSyn aggregation (patent #8,450,481) (43, 44). This report demonstrates the therapeutic effect of antiaggregation compounds in patient iPSC-derived neurons that not only improved their basal neuropathological features but also restored the neuronal network after proteasome inhibition, suggesting a positive impact even under conditions of increased cellular stress. NPT100-18A, which is most effective in patient neurons (Figs. 6 and 7), has been recently shown by Masliah and coworkers (43) to reduce αSyn toxicity in transgenic rodent models through a mechanism that involves αSyn displacement from the membrane. Hence, in the absence of isogenic gene-corrected control lines, the protective effects of these small molecules provide a direct link between the disease-associated phenotypes identified here and pathological αSyn. Most important, our data on patient iPSC-derived neurons uniquely demonstrate that targeting αSyn is a feasible therapeutic approach for developing new disease-modifying treatments for PD and other synucleinopathies.

An important observation is the endogenous dysregulation in p.A53T PD neurons, most notably down-regulation, of genes involved in various neuronal processes such as axon growth and transport, differentiation and maturation, and synaptic signaling. The presynaptic molecules altered included synapsin III (SYN3), a high-affinity αSyn interactor that has been found to colocalize with αSyn in the caudate-putamen of patients with PD (49) and to work cooperatively with αSyn to regulate synaptic function in dopaminergic neurons. SV2C, a molecule that also colocalizes with αSyn in synaptic puncta (50) and is involved in synaptic vesicle recycling (51), was also misrepresented. Additionally, genes such as DOC2B, a Ca^{2+}-dependent protein involved in vesicle trafficking, and RPH3A, a synaptic vesicle fusion molecule, were found diminished in PD neurons. The majority of presynaptic genes in our study exhibited decreased expression, a finding that confirms the loss of critical presynaptic proteins and the deficits in neurotransmitter release previously described in transgenic mice overexpressing human αSyn (52). Within the same

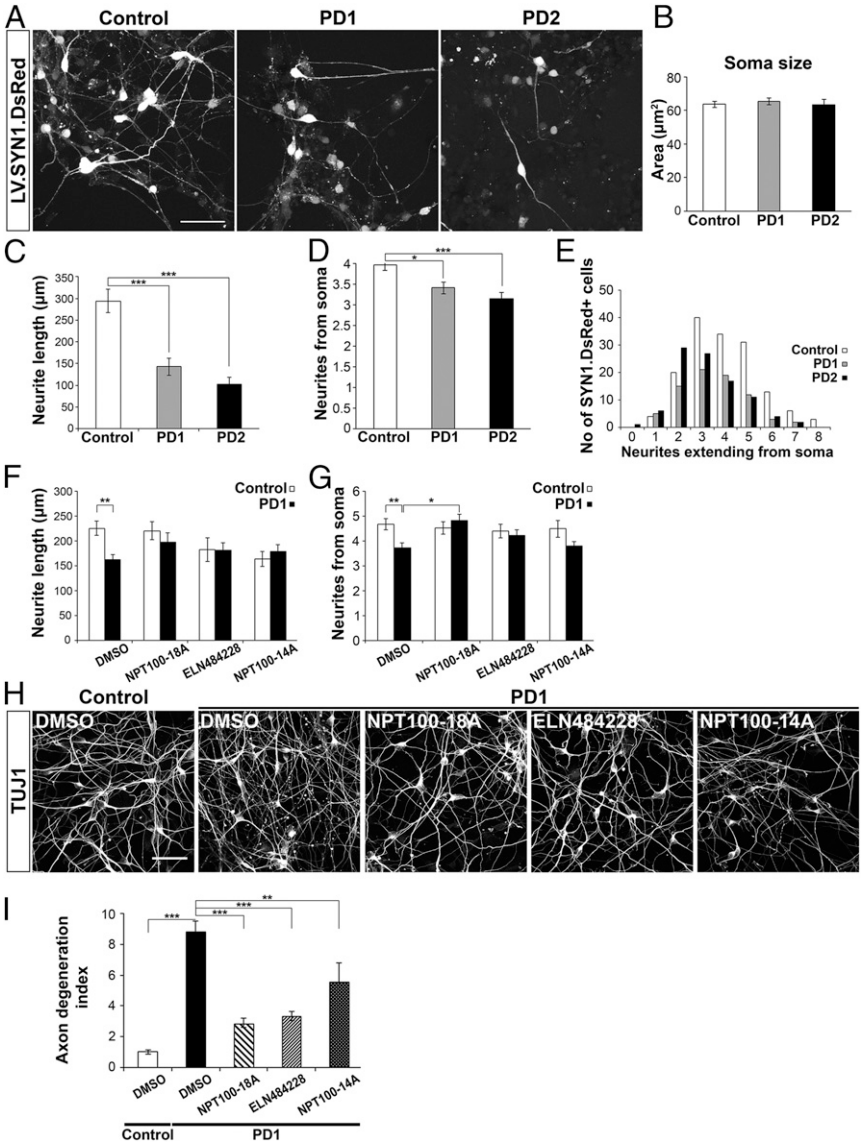

Fig. 6. Reversal of the neuropathological phenotype of PD iPSC-derived neurons by small molecules targeting αSyn. (*A*) Neurite analysis. Representative fluorescent images of iPSC-derived neurons at 50 DIV transduced with a lentiviral vector expressing red fluorescent protein DsRed under the control of the human synapsin 1 promoter (LV.SYN1.DsRed). (Scale bar, 40 μm.) Quantification of soma size (*B*), neurite length (*C*), and number of neurites extending from the soma (*D* and *E*) in SYN1.DsRed-positive cells. Data represent mean ± SEM (one-way ANOVA, $*P < 0.05$, $***P < 0.001$, n = at least 100 single DsRed-labeled neurons for each cell line). (*F* and *G*) Quantification of neurite length (*F*) and the number of neurites extending from the soma (*G*) of SYN1.DsRed-positive cells in control and PD1 neurons without treatment (DMSO) and after exposure to NPT100-18A, ELN484228, and NPT100-14A (2 nM). Data represent mean ± SEM (Student's t test for control–DMSO vs. PD1–DMSO, $**P < 0.01$, one-way ANOVA for control–DMSO vs. control–compounds and for PD1–DMSO vs. PD1–compounds, $*P < 0.05$, n = at least 100 single DsRed-labeled neurons for each condition). (*H*) Axonal pathology observed by TUJ1 immunostaining in PD1 cells is significantly improved by compound treatment. (Scale bar, 40 μm.) (*I*) Quantification of axonal degeneration by measuring the ratio of $TUJ1^+$ spots over the total $TUJ1^+$ area in untreated (DMSO) or compound-treated PD1 iPSC-derived neurons. Data represent mean ± SEM (one-way ANOVA, $**P < 0.01$, $***P < 0.001$, $n = 20$ randomly selected fields for each condition).

context, Scott et al. (52) have shown that overexpression of αSyn in cultured hippocampal neurons promotes a reduction in the levels of synaptic proteins at presynaptic terminals, a phenomenon termed "vacant synapses." Moreover, studies in sporadic and experimental Parkinson's disease suggest abnormalities in axonal transport proteins and alterations in synaptic activity (53, 54). Future experiments should associate the altered gene expression demonstrated here with disturbances in protein levels.

The postsynaptic side of the synapse and its complex molecular composition largely depend on signals received from the presynaptic terminal. Correspondingly, PD neurons exhibited significant changes in the expression of various postsynaptic molecules, including DLGAP2, GRIND2, and GRIP2. DLGAP2 is a membrane-bound synapse organizer the rare mutations of which are associated with autism (55), and GRIN2D and GRIP2 are components of the excitatory synapse. Furthermore, p.A53T-αSyn expression in iPSC-derived neurons affected greatly synaptic cell-adhesion molecules, required to mediate synaptic contact and alignment for proper synaptogenesis and maturation. From those cell-adhesion molecules, a striking number of the cadherin/proto-cadherin family members (40) had reduced expression, including CDH13 and CDH15, which are strongly linked to autism (56). Other autism-associated genes identified with diminished expression in PD neurons are the three members of the postsynaptic Slit- and Trk-like protein

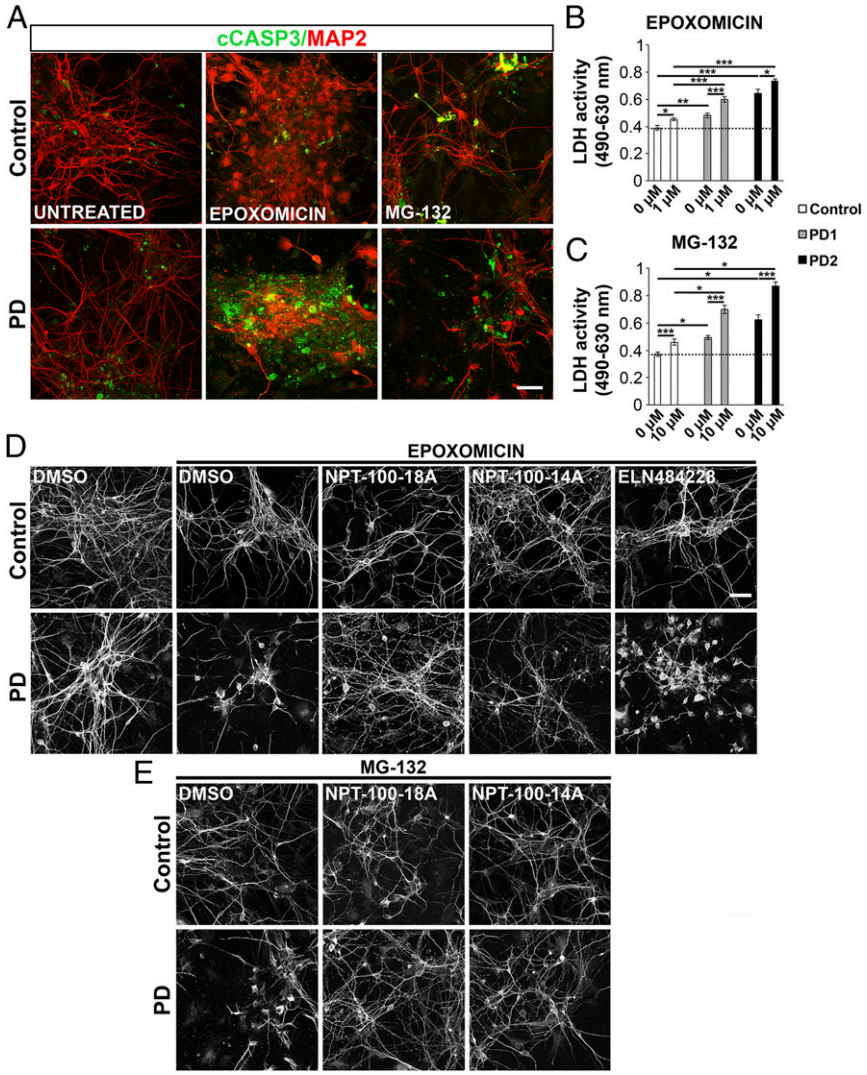

Fig. 7. Rescue of the cytotoxic effect of proteasome inhibition on PD iPSC-derived neurons. (*A*) Representative images of control and PD iPSC-derived neurons (55 DIV) immunostained for active cleaved caspase 3 (green) and MAP2 (red) after 24 h incubation with or without the proteasome inhibitors epoxomicin (1 μM) and MG-132 (10 μM). (Scale bar, 40 μm.) (*B* and *C*) Quantification of LDH activity (490–630 nm) in the culture supernatant as a measure of cytotoxicity in cells treated with epoxomicin (*B*) or MG-132 (*C*) under the same conditions as above. Data represent mean ± SEM from LDH activity in supernatants derived from 4 to 32 wells of four to six independent experiments performed in neurons derived from two iPSC lines from each subject (one-way ANOVA or ANOVA in Ranks for between-group comparisons followed by Dunn's test or Holm–Sidak for pairwise comparisons, $*P < 0.05$, $***P < 0.001$). (*D* and *E*) Induced-cytotoxicity experiments in iPSC-derived neurons (55–57 DIV) untreated (DMSO) or treated with small-molecule inhibitors of αSyn aggregation NPT100-18A, NPT100-14A, and ELN484228 (2 μM). Representative fluorescent images show TUJ1-positive neuronal network in DMSO and compound-treated cells after (*D*) epoxomicin (1 μM) or (*E*) MG-132 (10 μM) addition for 24 h. (Scale bar in *D*, 40 μm.)

family, SLITRK1, -2, and -4, all promoting excitatory synapse formation through binding to presynaptic protein tyrosine phosphatases (38, 57). Because neuronal communication depends on the formation of trans-synaptic adhesion complexes, their misrepresentation in PD neurons points to defective synaptogenesis. Indeed, PD neurons transduced with LV.SYN1.DsRed showed impaired neuritic growth, whereas PD neurons left to mature up to 100 d on an astrocytic feeder layer had significantly reduced synaptic contacts. The molecular and cellular phenotypes recognized in our study were corroborated by initial electrophysiological observations indicating changes in functional synaptic connectivity that deserve further investigation.

Defects in synaptogenesis and dysfunction in neuronal communication form the basis for neurodevelopmental disorders and a common feature of neurological diseases (58). Our data support the hypothesis that common mechanisms may operate in neurons in these diverse pathologies that may be activated by the presence of pathological αSyn and/or other aggregated proteins (59–61). This is an intriguing hypothesis, especially in the light of recent epidemiological findings that high rates of Parkinsonism are diagnosed in adults with autism (62).

There are currently no effective treatments for PD. Here, we have used iPSC technology to generate a cellular model that simulates key neuropathological features of the human disease with robust and reproducible phenotypes in patient-derived neurons. We reveal previously unrecognized impaired synaptic connectivity in p.A53T neurons and axonal neuropathology that could be reverted by small molecules targeting αSyn. Given the urgent need for effective drug development, our approach provides a basis for attempting such strategies to treat PD and other synucleinopathies. Furthermore, our cellular model, which has uncovered mechanistic insights into disease pathophysiology, is a powerful tool

for functional analyses and can serve as a platform for identification and testing of innovative disease-modifying compounds.

Materials and Methods

Extended experimental procedures are described in *SI Appendix, SI Materials and Methods*.

Study Approval. All procedures for generation of human iPSCs were approved by the Scientific Council and Ethics Committee of Attikon University Hospital (Athens, Greece), which is one of the Mendelian forms of Parkinson's Disease clinical centers, and by the Hellenic Pasteur Institute Ethics Committee overlooking stem cell research. Informed consent was obtained from all donors before skin biopsy.

Data and Materials Availability. RNA-seq data have been deposited in the Gene Expression Omnibus database under accession code GSE84684.

ACKNOWLEDGMENTS. We thank Prof. Fred Gage (Salk Institute for Biological Studies) for providing the plasmids for production of the lentiviral vector LV.SYN1.DsRed; Prof. Socrates Tzartos (Hellenic Pasteur Institute) for electrophysiology support; and Lina Florentin and Franci Sachinidi (Alpha Lab) for karyotype analysis. This work was supported by the following grants to R.M.: European Union FP7 REGPOT NEUROSIGN Project 264083; the Hellenic General Secretariat for Research and Technology Grants SYNERGASIA Noiseplus 09SYN-21-969 and ARISTEIA 2272 ParkinsonTransMed; the Fondation BNP Paribas; Empeirikion Foundation; the Fondation Santé; and the Institut Pasteur Grants PTR 417 and 523.

1. Lees AJ, Hardy J, Revesz T (2009) Parkinson's disease. *Lancet* 373:2055–2066.
2. Obeso JA, et al. (2010) Missing pieces in the Parkinson's disease puzzle. *Nat Med* 16: 653–661.
3. Schapira AH, Tolosa E (2010) Molecular and clinical prodrome of Parkinson disease: Implications for treatment. *Nat Rev Neurol* 6:309–317.
4. Braak H, Braak E (2000) Pathoanatomy of Parkinson's disease. *J Neurol* 247:II3–II10.
5. Bendor JT, Logan TP, Edwards RH (2013) The function of α-synuclein. *Neuron* 79: 1044–1066.
6. Dettmer U, et al. (2015) Corrigendum: Parkinson-causing α-synuclein missense mutations shift native tetramers to monomers as a mechanism for disease initiation. *Nat Commun* 6:8008.
7. Lashuel HA, Overk CR, Oueslati A, Masliah E (2013) The many faces of α-synuclein: From structure and toxicity to therapeutic target. *Nat Rev Neurosci* 14:38–48.
8. Simón-Sánchez J, et al. (2009) Genome-wide association study reveals genetic risk underlying Parkinson's disease. *Nat Genet* 41:1308–1312.
9. Petrucci S, Ginevrino M, Valente EM (2016) Phenotypic spectrum of alpha-synuclein mutations: New insights from patients and cellular models. *Parkinsonism Relat Disord* 22:S16–S20.
10. Chartier-Harlin MC, et al. (2004) Alpha-synuclein locus duplication as a cause of familial Parkinson's disease. *Lancet* 364:1167–1169.
11. Polymeropoulos MH, et al. (1997) Mutation in the alpha-synuclein gene identified in families with Parkinson's disease. *Science* 276:2045–2047.
12. Tieu K (2011) A guide to neurotoxic animal models of Parkinson's disease. *Cold Spring Harb Perspect Med* 1:a009316.
13. Devine MJ, et al. (2011) Parkinson's disease induced pluripotent stem cells with triplication of the α-synuclein locus. *Nat Commun* 2:440.
14. Ryan SD, et al. (2013) Isogenic human iPSC Parkinson's model shows nitrosative stress-induced dysfunction in MEF2-PGC1α transcription. *Cell* 155:1351–1364.
15. Chung CY, et al. (2013) Identification and rescue of α-synuclein toxicity in Parkinson patient-derived neurons. *Science* 342:983–987.
16. Schöndorf DC, et al. (2014) iPSC-derived neurons from GBA1-associated Parkinson's disease patients show autophagic defects and impaired calcium homeostasis. *Nat Commun* 5:4028.
17. Jiang H, et al. (2012) Parkin controls dopamine utilization in human midbrain dopaminergic neurons derived from induced pluripotent stem cells. *Nat Commun* 3:668.
18. Cooper O, et al. (2012) Pharmacological rescue of mitochondrial deficits in iPSC-derived neural cells from patients with familial Parkinson's disease. *Sci Transl Med* 4:141ra90.
19. Nabi R, Serajee FJ, Chugani DC, Zhong H, Huq AH (2004) Association of tryptophan 2,3 dioxygenase gene polymorphism with autism. *Am J Med Genet B Neuropsychiatr Genet* 125B:63–68.
20. Takahashi K, et al. (2007) Induction of pluripotent stem cells from adult human fibroblasts by defined factors. *Cell* 131:861–872.
21. Cowan CA, et al. (2004) Derivation of embryonic stem-cell lines from human blastocysts. *N Engl J Med* 350:1353–1356.
22. Chambers SM, et al. (2009) Highly efficient neural conversion of human ES and iPS cells by dual inhibition of SMAD signaling. *Nat Biotechnol* 27:275–280.
23. Soldner F, et al. (2009) Parkinson's disease patient-derived induced pluripotent stem cells free of viral reprogramming factors. *Cell* 136:964–977.
24. Spira PJ, Sharpe DM, Halliday G, Cavanagh J, Nicholson GA (2001) Clinical and pathological features of a Parkinsonian syndrome in a family with an Ala53Thr alpha-synuclein mutation. *Ann Neurol* 49:313–319.
25. Markopoulou K, et al. (2008) Clinical, neuropathological and genotypic variability in SNCA A53T familial Parkinson's disease. Variability in familial Parkinson's disease. *Acta Neuropathol* 116:25–35.
26. Papadimitriou D, et al. (2016) Motor and nonmotor features of carriers of the p.A53T alpha-synuclein mutation: A longitudinal study. *Mov Disord* 31:1226–1230.
27. Conway KA, Harper JD, Lansbury PT (1998) Accelerated in vitro fibril formation by a mutant alpha-synuclein linked to early-onset Parkinson disease. *Nat Med* 4:1318–1320.
28. Shen D, et al. (2011) Novel cell- and tissue-based assays for detecting misfolded and aggregated protein accumulation within aggresomes and inclusion bodies. *Cell Biochem Biophys* 60:173–185.
29. Kotzbauer PT, et al. (2004) Fibrillization of alpha-synuclein and tau in familial Parkinson's disease caused by the A53T alpha-synuclein mutation. *Exp Neurol* 187:279–288.
30. Duda JE, et al. (2002) Concurrence of alpha-synuclein and tau brain pathology in the Contursi kindred. *Acta Neuropathol* 104:7–11.
31. Zoghbi HY, Bear MF (2012) Synaptic dysfunction in neurodevelopmental disorders associated with autism and intellectual disabilities. *Cold Spring Harb Perspect Biol* 4:a009886.
32. Mirnics K (2011) Schizophrenia. Special issue introduction. *Int J Dev Neurosci* 29: 189–191.
33. Schloesser RJ, Huang J, Klein PS, Manji HK (2008) Cellular plasticity cascades in the pathophysiology and treatment of bipolar disorder. *Neuropsychopharmacology* 33:110–133.
34. Porton B, Wetsel WC, Kao HT (2011) Synapsin III: Role in neuronal plasticity and disease. *Semin Cell Dev Biol* 22:416–424.
35. Janz R, Südhof TC (1999) SV2C is a synaptic vesicle protein with an unusually restricted localization: Anatomy of a synaptic vesicle protein family. *Neuroscience* 94:1279–1290.
36. Burns ME, Sasaki T, Takai Y, Augustine GJ (1998) Rabphilin-3A: A multifunctional regulator of synaptic vesicle traffic. *J Gen Physiol* 111:243–255.
37. Friedrich R, et al. (2008) DOC2B acts as a calcium switch and enhances vesicle fusion. *J Neurosci* 28:6794–6806.
38. Yim YS, et al. (2013) Slitrks control excitatory and inhibitory synapse formation with LAR receptor protein tyrosine phosphatases. *Proc Natl Acad Sci USA* 110:4057–4062.
39. Sheng M, Kim E (2011) The postsynaptic organization of synapses. *Cold Spring Harb Perspect Biol* 3:a005678.
40. Arikkath J, Reichardt LF (2008) Cadherins and catenins at synapses: Roles in synaptogenesis and synaptic plasticity. *Trends Neurosci* 31:487–494.
41. Budnik V, Salinas PC (2011) Wnt signaling during synaptic development and plasticity. *Curr Opin Neurobiol* 21:151–159.
42. Südhof TC (2013) Neurotransmitter release: The last millisecond in the life of a synaptic vesicle. *Neuron* 80:675–690.
43. Wrasidlo W, et al. (2016) A de novo compound targeting α-synuclein improves deficits in models of Parkinson's disease. *Brain* 139:3217–3236.
44. Tóth G, et al. (2014) Targeting the intrinsically disordered structural ensemble of α-synuclein by small molecules as a potential therapeutic strategy for Parkinson's disease. *PLoS One* 9:e87133.
45. Kehagia AA, Barker RA, Robbins TW (2010) Neuropsychological and clinical heterogeneity of cognitive impairment and dementia in patients with Parkinson's disease. *Lancet Neurol* 9:1200–1213.
46. Chung CY, Koprich JB, Siddiqi H, Isacson O (2009) Dynamic changes in presynaptic and axonal transport proteins combined with striatal neuroinflammation precede dopaminergic neuronal loss in a rat model of AAV alpha-synucleinopathy. *J Neurosci* 29:3365–3373.
47. Spillantini MG, Crowther RA, Jakes R, Hasegawa M, Goedert M (1998) alpha-Synuclein in filamentous inclusions of Lewy bodies from Parkinson's disease and dementia with lewy bodies. *Proc Natl Acad Sci USA* 95:6469–6473.
48. Goedert M (2001) The significance of tau and alpha-synuclein inclusions in neurodegenerative diseases. *Curr Opin Genet Dev* 11:343–351.
49. Zaltieri M, et al. (2015) α-Synuclein and synapsin III cooperatively regulate synaptic function in dopamine neurons. *J Cell Sci* 128:2231–2243.
50. Busch DJ, et al. (2014) Acute increase of α-synuclein inhibits synaptic vesicle recycling evoked during intense stimulation. *Mol Biol Cell* 25:3926–3941.
51. Nemani VM, et al. (2010) Increased expression of alpha-synuclein reduces neurotransmitter release by inhibiting synaptic vesicle reclustering after endocytosis. *Neuron* 65:66–79.
52. Scott DA, et al. (2010) A pathologic cascade leading to synaptic dysfunction in alpha-synuclein-induced neurodegeneration. *J Neurosci* 30:8083–8095.
53. Chu Y, et al. (2012) Alterations in axonal transport motor proteins in sporadic and experimental Parkinson's disease. *Brain* 135:2058–2073.
54. Simunovic F, et al. (2009) Gene expression profiling of substantia nigra dopamine neurons: Further insights into Parkinson's disease pathology. *Brain* 132:1795–1809.
55. Chien WH, et al. (2013) Deep exon resequencing of DLGAP2 as a candidate gene of autism spectrum disorders. *Mol Autism* 4:26.
56. Redies C, Hertel N, Hübner CA (2012) Cadherins and neuropsychiatric disorders. *Brain Res* 1470:130–144.
57. Um JW, et al. (2014) Structural basis for LAR-RPTP/Slitrk complex-mediated synaptic adhesion. *Nat Commun* 5:5423.
58. Habela CW, Song H, Ming GL (2016) Modeling synaptogenesis in schizophrenia and autism using human iPSC derived neurons. *Mol Cell Neurosci* 73:52–62.
59. Jellinger KA (2009) Lewy body/alpha-synucleinopathy in schizophrenia and depression: A preliminary neuropathological study. *Acta Neuropathol* 117:423–427.
60. Korth C (2012) Aggregated proteins in schizophrenia and other chronic mental diseases: DISC1opathies. *Prion* 6:134–141.
61. Atkin TA, Brandon NJ, Kittler JT (2012) Disrupted in Schizophrenia 1 forms pathological aggresomes that disrupt its function in intracellular transport. *Hum Mol Genet* 21:2017–2028.
62. Starkstein S, Gellar S, Parlier M, Payne L, Piven J (2015) High rates of parkinsonism in adults with autism. *J Neurodev Disord* 7:29.

Supporting Information

SI Material and Methods

Generation and characterization of human iPSCs. Skin fibroblasts from two PD patients (PD1 and PD2) carrying the G209A (p.A53T) SNCA mutation and one unaffected subject (Table S1A) were obtained from the Biobank generated within the context of the European Project on Mendelian Forms of Parkinson's Disease (MEFOPA). Fibroblasts were cultured in Dulbecco's modified Eagle's medium (DMEM, Life Technologies) supplemented with 10% fetal bovine serum (FBS, Life Technologies), 2mM GlutaMax (Life Technologies) and 1% penicillin/streptomycin (Life Technologies). iPSCs were generated by transduction of human fibroblasts with retroviral vectors expressing the human cDNAs of OCT4, SOX2, KLF4 and C-MYC, as previously described (1). Colonies of iPSCs were manually picked after 3-5 weeks for further expansion and characterization. Two iPSC lines from each individual were used for further characterization, differentiation and functional studies (Table S1A). iPSCs were cultured on irradiated mouse embryonic fibroblasts (MEFs, Globalstem) in iPSC medium consisting of KnockOut DMEM (KO-DMEM, Life Technologies), 20% Knockout Serum Replacement (KSR, Life Technologies), 2 mMGlutaMax, MEM Non-Essential Amino Acids (100x MEM NEAA, Life Technologies), 100 mM β-mercaptoethanol (Life Technologies) and 10 ng/ml human basic FGF (bFGF, Miltenyi). For feeder-free culture, cells were cultured on Geltrex (Life Technologies) with Essential 8 basal medium (Life Technologies). Medium was changed daily and cells were passaged as small clumps using collagenase (1 mg/ml; Life Technologies) or an enzyme-free reagent (ReLeSR, StemCell Technologies) every 3 to 6 days. Karyotype analysis was performed using standard G-banding technique. Pluripotency*in vitro* was assessed by embryoid body (EB) formation and spontaneous

differentiation. iPSCs were seeded in non-tissue culture treated dishes (ultra-low attachment) with iPSC medium without bFGF (EB medium). After 8 days in suspension, EBs were transferred to gelatin-coated dishes containing the same medium for an additional 10–25 days. Teratoma formation assay was performed to assess *in vivo*pluripotency of iPSC lines. iPSCs were mixed with matrigel (v/v 1:1) and injected subcutaneously into the dorsal flank of NOD/SCID mice. Seven weeks post-injection, the mice were sacrificed and the tumors were surgically removed. The tumors were then fixed in 10% formalin, embedded in paraffin, sectioned at 4 μm and stained with hematoxylin and eosin. The characterization of generated iPSCs was performed in comparison with HUES6 cell line (2).

Neuronal differentiation of human iPSCs. A schematic summary of the differentiation procedure is shown in Fig. S1. iPSC colonies were dissociated with accutase (Life Technologies) for 10 min and re-suspended in EB medium supplemented with 10 μM ROCK inhibitor Y-27632 (Tocris Bioscience). After 5 days DIV, neural induction was achieved by dual suppression of the SMAD signaling pathway (3) using a combination of Noggin (250 ng/ml; R&D Systems) and SB431542 (10 μM; Tocris Bioscience) in DMEM: F12/N2-medium (Neural induction medium) for 8 DIV to generate neural precursor cells (NPCs). For neuronal differentiation, NPCs were dissociated with accutase and plated onto poly-L-ornithine (PLO; 20 μg/ml; Sigma-Aldrich)/ laminin (5 μg/ml; Sigma-Aldrich)-coated coverslips (Passage 1; P1) in Neurobasal/ B27/N2-medium supplemented with 200 ng/ml human recombinant sonic hedgehog (SHH, R&D Systems) and 100 ng/ml murine recombinant fibroblast growth factor 8b (FGF-8b, R&D Systems) for 8 DIV, followed by a cocktail consisting of 20 ng/ml brain-derived neurotrophic factor (BDNF, R&D

Systems), 10 ng/ml glial cell-derived neurotrophic factor (GDNF, R&D Systems), 200 μM ascorbic acid (AA, Sigma-Aldrich) and 0.5 mM cyclic AMP (cAMP, Sigma-Aldrich) for at least 3 weeks (4). Half of the medium was replaced every other day. After 30-35 DIV of neuronal differentiation, corresponding to a total of 43-48 DIV, cells were either harvested for RNA and protein extraction or re-plated (P2) onto PLO/laminin-coated coverslips for phenotypic, electrophysiological and biochemical analysis (Fig. S1). For long-term culture maintenance (up to 100 days) cells were seeded on mouse primary astrocytes (Fig. S1).

Electrophysiology. Whole-cell voltage and current-clamp recordings were performed on iPSC-derived neurons at 55-70 DIV that had been re-plated on PLO/laminin-coated coverslips. Cells were visualized on an inverted microscope (Olympus CKX41). Pipette resistance was 3-7 MΩ. The extracellular solution contained (mM): 140 NaCl, 2.8 KCl, 2 CaCl2, 4 MgCl2, 20 HEPES, 10 glucose, pH 7.4-7.5, Osm 320-330 mOsml/l. The patch pipette solution contained (mM): 140 KCl, 1 CaCl2, 2 MgCl2, 10 HEPES, 5 EGTA, 2 MgATP, 0.4 N2GTP, pH 7.2-7.3, Osm 280-290 mOsml/l. For recording of voltage-gated sodium and potassium currents, voltage steps ranging from -80 mV to +50 mV were delivered at 10 mV increments. For rapid replacement of solutions, a system of two parallel rectangular tubes, 100 μm in diameter, located at a distance of 40-50 μm from the tested cell, was used. The movement of tubes was controlled by a computer-driven fast exchange system (SF 77A Perfusion Fast-Step, Warner, USA). The pharmacological inhibitors tetrodotoxin (TTX; final concentration 1 μM) and tetraethylammonium (TEA; 20 mM) were applied to block voltage-gated sodium and potassium channels, respectively. GABA, glutamate, nicotine and glycine were applied at 3 different concentrations (10, 100

and 1000 μM). For current protocols, cells were current-clamped at their resting membrane potential (0 pA) and a depolarizing current was applied (+40 pA). Data were acquired at room temperature (22-24°C) using an EPC9 HEKA amplifier and an ITC-16 acquisition system with a patchmaster software (HEKA). Data analysis was performed using OriginPro 8 (OriginLab Software).

Genome-wide RNA sequencing and bioinformatics analysis. Total cellular RNA was extracted from the following samples and sequenced on an Illumina HiSeq sequencer at the European Molecular Biology Laboratory (EMBL): PD1 and control skin fibroblasts, PD1 and control iPSCs (two lines each; PD1-1/PD1-2 and C1-1/C1-2) and from each iPSC line the derived NPCs and neurons, along with HUES 6, HUES 6-derived NPCs and HUES-derived neurons. RNA libraries were prepared with the TruSeq RNA Sample Preparation Kit V2 (Illumina). Raw RNA-seq reads were quality checked using FastQC (www.bioinformatics.babraham.ac.uk/projects/fastqc/). Contaminants were detected and removed utilizing a combination of an in-house-developed algorithm and already available tools (5). Following pre-processing, GSNAP spliced aligner (6) was utilized to map the RNA-seq reads against the reference genome (GRCh37/hg19 genome assembly). GSNAP has been appropriately parameterized in order to detect novel and known splice junctions. Differential expression analysis was performed using DESeq (7). Heat maps were implemented using R/Bioconductor (8, 9) (Clustering: Pearson's correlation coefficient, row-wise scaling: centering and scaling using Z-scores). Enrichment analyses were performed against Gene Ontology10 using the hypergeometric distribution, KEGG and Reactome pathway databases. All gene annotations were derived from Ensembl (10).

Genomic DNA analysis for detection of the p.A53T (G209A) mutation. Genomic DNA of fibroblasts and iPSCs was extracted by NucleoSpin Tissue Kit (Macherey-Nagel) following the manufacturer's recommended protocol. Specific primers were used for SNCA gene (Table S2A) and PCR products were digested by the restriction enzyme Tsp45I (New England Biolabs). p.A53T (G209A) mutation results in a novel Tsp45I site and two additional fragments of 128 and 88 bp can be detected.

RNA isolation, cDNA Synthesis and qPCR. Total RNA was extracted from cell pellets using the TRIzol® Reagent (Life Technologies). Following digestion with DNase I, 1 μg of total RNA was used for first strand cDNA synthesis with the ImProm-II Reverse Transcription System (Promega) according to the manufacturer's instructions. Quantitative PCR analyses were carried out in a Light Cycler 96 (Roche) Real time PCR detection system using KAPA SYBR FAST qPCR Master Mix (KapaBiosystems). All primers used are listed in Table S2A.

Immunofluorescence staining. Cells were fixed with 4% paraformaldehyde (Sigma-Aldrich) for 20 min at room temperature. Samples were blocked with 0.1% Triton X-100 (Sigma-Aldrich) and 5% donkey serum in PBS for 30 min and were subsequently incubated with primary antibodies (Table S2B) at 4^{o}C overnight, followed by incubation with appropriate secondary antibodies (Molecular Probes, Thermo Fisher Scientific) conjugated to AlexaFluor 488 (green) or 546 (red), for at least 1 h at room temperature. For detection of phosphorylated αSyn (Ser129) cells were permeabilized with 0.1% Triton X-100 for 5 min and blocked with 3% BSA in PBS for 30 min. Protein aggregates were detected with 0.05% Thioflavin S solution (Sigma, in 70%

ethanol) or with the PROTEOSTAT Aggresome Detection Kit (Enzo) followed by immunolabeling for αSyn. Coverslips were mounted with ProLong Gold antifade reagent with DAPI (Cell Signaling) and images were acquired using a Leica TCS-SP5II confocal microscope (LEICA Microsystems) and analyzed using ImageJ software (NIH).

Western blot. Control, PD1 and PD2 neuronal cultures were lysed at 4^{o}C for 15 min in ice cold lysis buffer [150mMNaCl, 50 mM Tris, 2mM EDTA 1%v/v Triton X-100 (pH 7.6) containing PhosSTOP phosphatase inhibitors and a complete protease inhibitor mixture (Roche Life Science)], sonicated and centrifuged at 20,000 *g*. Protein concentration was estimated in the supernatant by Bradford assay (Applichem). Samples (50 μg) were loaded onto 4-12% gradient NuPAGEBis-Tris precast mini gel (Life Technologies) and after electrophoresis proteins were transferred onto 0.20 μm pore size nitrocellulose membrane (Maine Manufacturing, Nitrobind, Cast, Pure). The membrane was heated at 65^{o}C, overnight in PBS. Non-specific binding sites were blocked in TBS/ 0.1% Tween 20/ 5% skimmed milk for 1 hour at 20 ^{o}C followed by overnight incubation with mouse anti-αSyn (1:1000; BD Biosciences), rabbit anti-phosphorylated αSyn (Ser129) (1:1000; Abcam) or mouse anti-GAPDH (1:1000; Santa Cruz Biotechnology) diluted in TBS/ 0.1% Tween 20/3% BSA or in TBS/ 0.1% Tween 20/ 2.5% skimmed milk. Incubation with appropriate HRP-conjugated secondary antibodies (Thermo) was performed for 2 hours at room temperature and protein bands were visualized using the Amersham ECL Prime Western Blotting Detection Reagent (GE Healthcare). The experiment was performed twice.

Production of SYN1.DsRed lentiviral vector. Four plasmids (provided by Dr. Fred Gage, The Salk Institute for Biological Studies) were used for the production of the lentiviral vector expressing protein DsRed red fluorescent protein under the control of the human synapsin 1 promoter (LV.SYN1.DsRed): the lentiviral transfer vector and three lentiviral packaging vectors (pMDL, pRev and pVSVG). The preparation and purification of the lentiviral vector was performed as previously described (11). LV.SYN1.DsRed was used for transduction of human cells either in the beginning of neuronal differentiation or after re-plating (Fig. S1), in order to facilitate imaging of single neurons for morphological analysis.

Neurite analysis. Neurite analysis was performed on re-plated iPSC-derived neurons at 50-60 DIV. Transduction with LV.SYN1.DsRed was performed at least 7 days before the assay to depict and count branching neurites from single neurons. The number of neurites extending from the soma of at least 100 single DsRed-labelled neurons per sample was determined. Neurite length was estimated by manually tracing the length of all neurites on DsRed-labelled neurons using the NeuronJ plugin of ImageJ (NIH).

Axon degeneration index. Analysis of axonal degeneration was performed by immunostaining for βIII-tubulin (TUJ1) in iPSC-derived control and PD neuronal cultures. The cultures were either untreated (in the presence of DMSO) or treated with NPT100-18A, ELN484228, NPT100-14A (in the case of PD cultures). The number of TUJ1+ spots in blebbed or fragmented axons was counted manually (ImageJ) on twenty randomly selected fields and the ratio between the number of spots and the total TUJ1+ staining area (ImageJ) was defined as axon degeneration index.

Primary culture of mouse astrocytes. Astrocytes were purified from neonatal P0-P1 mouse cortices and plated in DMEM/10% FCS in poly-D-lysine (PDL)-coated tissue culture flasks as previously described (12). When confluent, the flasks with adherent cells were shaken in an orbital shaker at 120 rpm, over 20 h at 37^{o}C to remove microglia and oligodendrocyte progenitor cells, resulting in approximately 95% astrocyte purity as determined by GFAP immunostaining. Astrocytes were then detached by incubation with trypsin/EDTA, re-plated on PLO/laminin-coated coverslips and allowed to reach confluence for about one week. This astrocytic feeder layer was used for co-culture with human iPSC-derived neurons.

Synapse density. Synaptic protein staining was performed on 70 and 100 DIV iPSC-derived neurons seeded on mouse astrocytes. The total SYN1/PSD95 puncta pairs were counted manually using ImageJ, in order to assess the synaptic contact density. The synaptic density was determined as the number of SYN1/PSD95 pairs per 10 μm neurite length. Neurites were traced using the NeuronJ plugin (ImageJ).

Cytotoxicity Assays. Control and PD neurons from parallel re-plated cultures at 50-60 DIV were subjected to stress by adding epoxomicin (Sigma-Aldrich) and MG-132 (Calbiochem, Merck-Millipore) for 24 h. Cell cytotoxicity (Cytotoxicity Detection Kit, LDH; Roche) was determined in cultures in 24 hours after stressor addition, according to the manufacturer's protocol.

Treatment with small-molecule inhibitors of αSyn aggregation. Three *de novo in silico* designed compounds, namely NPT100-18A (13), NPT100-14A (Patent # 8,450,481) and ELN484228 (14) (provided by Prof. E. Masliah, UC San Diego, CA,

USA), resuspended in DMSO, were added in the culture medium since the onset of neural differentiation at 2 nM. Treated control and PD1 cultures with either compounds or DMSO as vehicle were used for neurite analysis as well as for induced-stress experiments and cytotoxicity assays.

Statistics. All experiments were replicated at least three times and data from parallel cultures were acquired. All data represent mean±standard error of mean (SEM). Statistical analysis was performed using Minitab 17. Comparisons between two independent groups were performed using Student's t-test. One-way ANOVA with Tukey's post hoc test was utilized for multiple group comparisons. The statistical analysis of cytotoxicity experiments was performed using SigmaStat 4.0 (Systat Software, Inc). ANOVA on Ranks followed by Dunn's test was performed for all concurrent analyses of multiple groups, where comparisons of independent samples from different samples sizes were incorporated. For parametric data, one-way ANOVA was performed followed by Holm-Sidak correction for pairwise comparisons. Probability values less than 0.05 ($p < 0.05$) were considered significant.

References

1. Takahashi K, et al. (2007) Induction of pluripotent stem cells from adult human fibroblasts by defined factors. *Cell* 131(5):861-872.
2. Cowan CA, et al. (2004) Derivation of embryonic stem-cell lines from human blastocysts. *N Engl J Med* 350(13):1353-1356.
3. Chambers SM, et al. (2009) Highly efficient neural conversion of human ES and iPS cells by dual inhibition of SMAD signaling. *Nat Biotechnol* 27(3):275-280.

4. Soldner F, et al. (2009) Parkinson's disease patient-derived induced pluripotent stem cells free of viral reprogramming factors. *Cell* 136(5):964-977.
5. Georgakilas G, et al. (2014) microTSS: accurate microRNA transcription start site identification reveals a significant number of divergent pri-miRNAs. *Nat Commun* 5:5700.
6. Wu TD & Nacu S (2010) Fast and SNP-tolerant detection of complex variants and splicing in short reads. *Bioinformatics* 26(7):873-881.
7. Anders S & Huber W (2010) Differential expression analysis for sequence count data. *Genome Biol* 11(10):R106.
8. Gentleman RC, et al. (2004) Bioconductor: open software development for computational biology and bioinformatics. *Genome Biol* 5(10):R80.
9. R CORE TEAM A (2012) R: A language and environment for statistical computing. R Foundation for Statistical Computing, Vienna, Austria. 2012. (ISBN 3-900051-07-0, URL http://www. R-project. org).
10. Yates A, et al. (2016) Ensembl 2016. *Nucleic Acids Res* 44(D1):D710-716.
11. Tiscornia G, Singer O, & Verma IM (2006) Production and purification of lentiviral vectors. *Nat Protoc* 1(1):241-245.
12. Papastefanaki F, et al. (2007) Grafts of Schwann cells engineered to express PSA-NCAM promote functional recovery after spinal cord injury. *Brain* 130(Pt 8):2159-2174.
13. Wrasidlo W, et al. (2016) A de novo compound targeting alpha-synuclein improves deficits in models of Parkinson's disease. *Brain* in press.
14. Toth G, et al. (2014) Targeting the intrinsically disordered structural ensemble of alpha-synuclein by small molecules as a potential therapeutic strategy for Parkinson's disease. *PLoS One* 9(2):e87133.

SI Figures

Figure S1

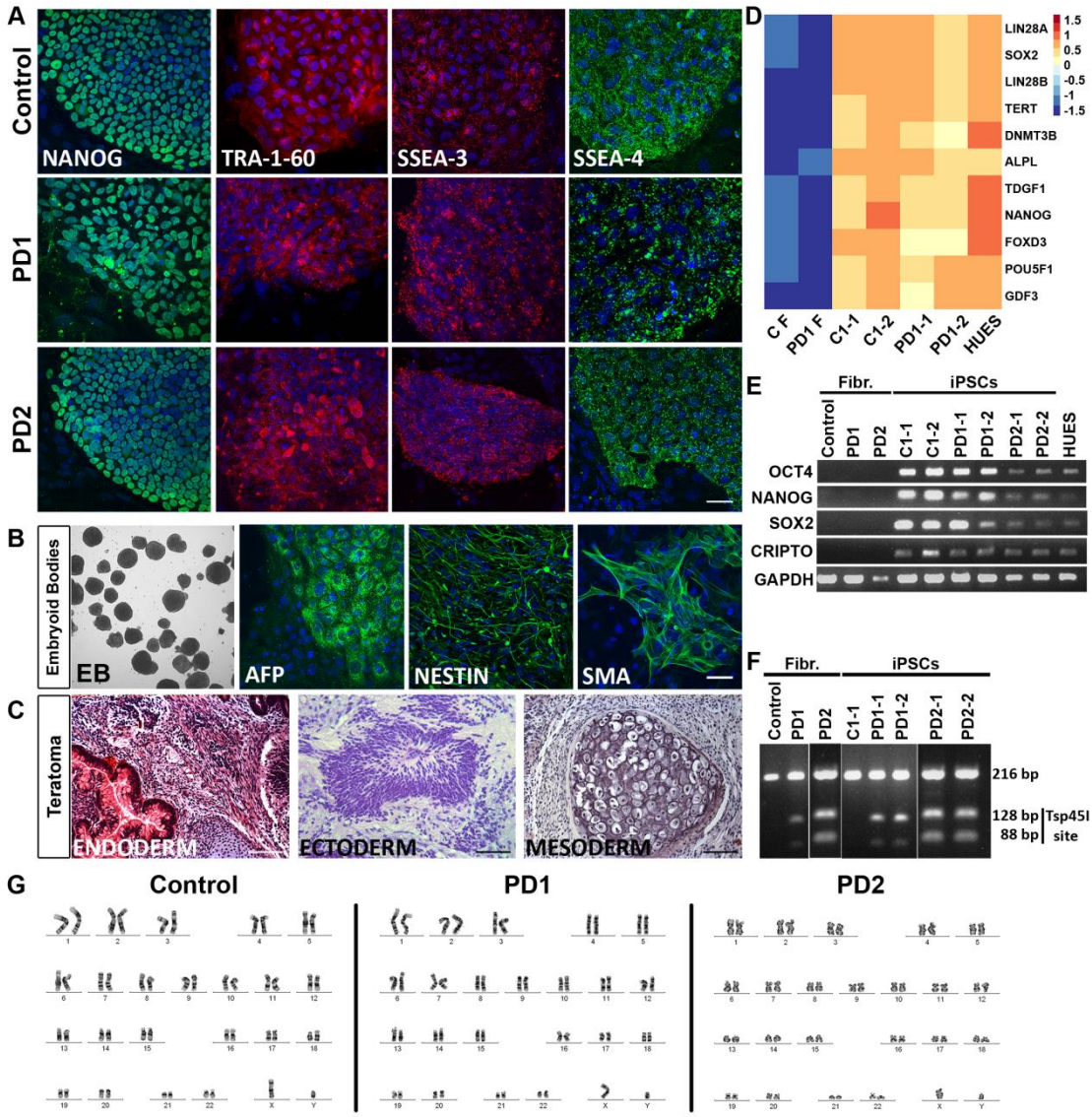

Figure S1. Generation of iPSCs. (**A**) Representative micrographs of iPSCs derived from two PD patients (PD1, PD2) and one unaffected individual (Control) expressing pluripotency markers Nanog, Tra-1-60, SSEA3 and SSEA4. Scale bar, 40 µm. (**B**) Embryoid bodies (EBs, brightfield) consisting of cells (fluorescent images) of endodermal (α-fetoprotein, AFP), ectodermal (Nestin) and mesodermal (smooth muscle actin, SMA) origin under spontaneous differentiation conditions *in vitro*. Scale bar, 20 µm. (**C**) *In vivo*teratoma formation after iPSC injection into immune-

compromised mice with evidence of all three germ layers. Scale bars, 100, 50 and 100 μm, respectively. (**D, E**) Gene expression heat map (**D**) and RT-PCR (**E**) showing the expression of selected pluripotency genes in generated iPSCs and HUES.(**F**) Genomic DNA analysis demonstrating the presence of the heterozygous G209A SNCA mutation in PD skin fibroblasts and PD-iPSCs but not in control cells. (**G**) Representative data of karyotype analysis in one line of control, PD1 and PD2 iPSCs.

Figure S2

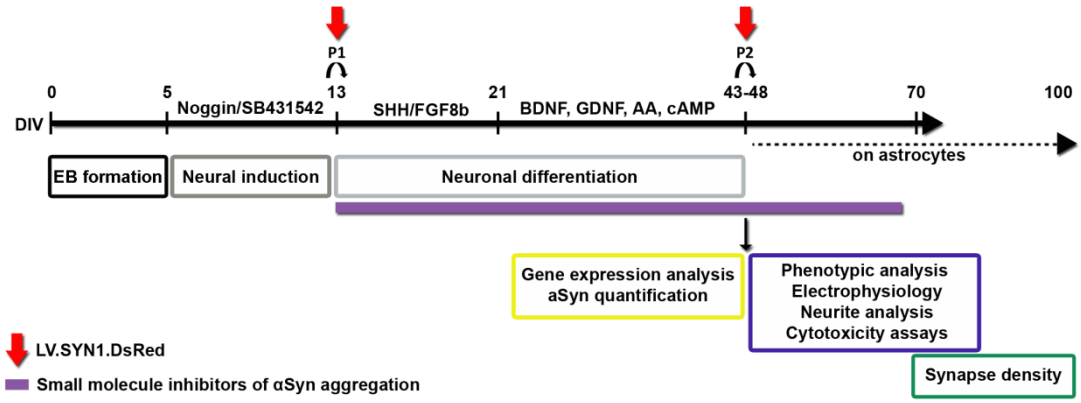

Figure S2. Schematic drawing of the protocol used for neuronal differentiation of iPSCs and timeline of analysis. Embryoid body (EB) formation (5 DIV) was followed by dual-SMAD inhibition using Noggin and SB431542 for neural induction and generation of neural precursor cells (8 DIV). Dissociated cells were then plated (Passage 1; P1) onto PLO/laminin-coated coverslips and neuronal differentiation was initiated in the presence of sonic hedgehog (SHH) and fibroblast growth factor 8b (FGF-8b) for 8 days. For neuron maturation, brain-derived neurotrophic factor (BDNF), glial cell-derived neurotrophic factor (GDNF), ascorbic acid (AA) and cyclic AMP (cAMP) were added for at least 3 weeks. At 43-48 DIV cells were either harvested for gene expression analysis and αSyn protein quantification or were re-plated (P2) onto PLO/laminin-coated coverslips for phenotypic characterization, electrophysiological studies, neurite analysis and cytotoxicity assays (up to 70 DIV). Long-term culture maintenance up to 100 DIV was achieved by seeding iPSC-derived neurons on mouse primary astrocytes (dashed line) in order to assess synapse contact density. Transduction with a lentiviral vector expressing the DsRed protein under the human synapsin 1 promoter (LV.SYN1.DsRed) was performed at 13 DIV or 43-48 DIV (red arrows) to image and count branching neurites from single neurons. Small molecule inhibitors of αSyn aggregation were applied throughout neuronal differentiation and maturation (purple bar) to assess rescue of disease phenotypes.

Figure S3

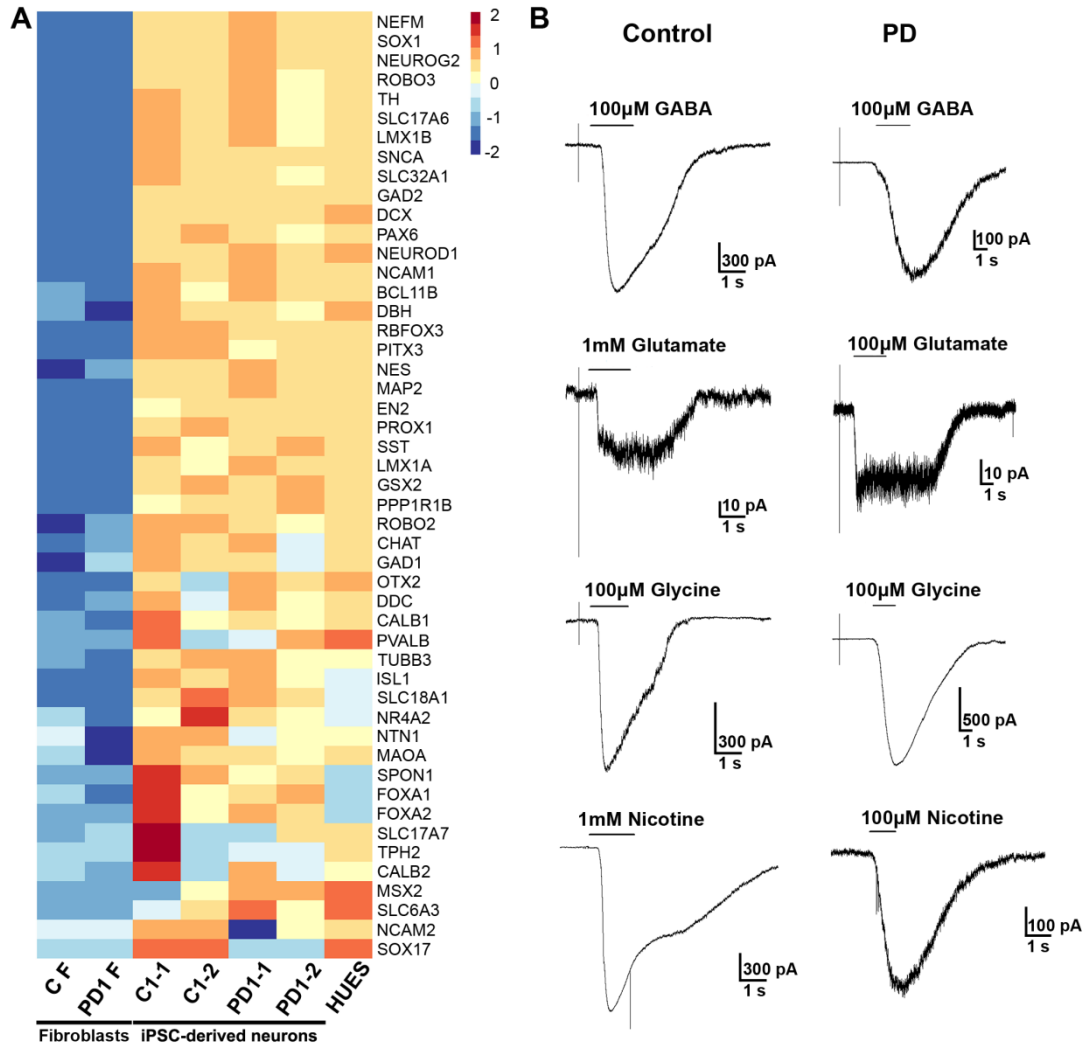

Figure S3. Gene expression heat map for selected genes and neurotransmitter-evoked electrophysiological responses of iPSC-derived neurons. (**A**) Gene expression heat map showing immature and mature neuronal markers in both control and PD1 iPSC-derived neurons. (**B**) Representative traces of ionic currents induced by application of the neurotransmitters GABA, glutamate, glycine and nicotine. Membrane potential was held at -70 mV. Bars above traces indicate the time of agonist application.

Figure S4

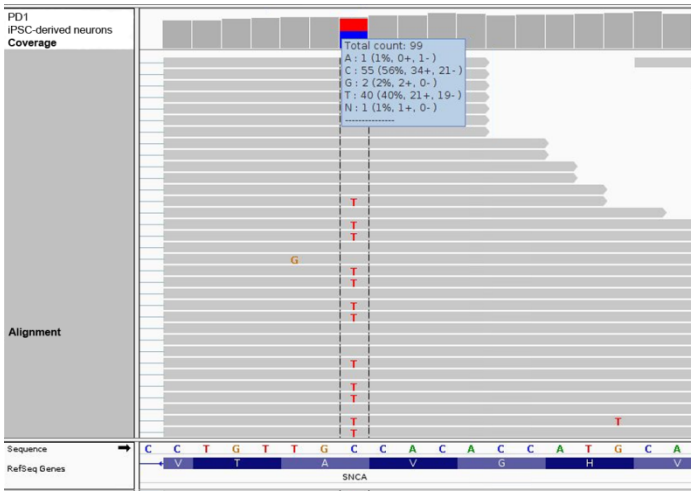

Figure S4. Expression of the mutant SNCA allele in PD iPSC-derived neurons. Screenshot from Integrated Genome Viewer (IGV) depicting the RNA-seq coverage of PD1 iPSC-derived neurons at the p.A53T/G209A mutation locus (ENSP00000422238.1:p.Ala53Thr). The browser depicts the region chr4: 90749293-90749311 (GRCh37). The variant is covered by 99 reads, with 40 reads bearing the mutated allele. The event is marked in the browser as a C to T mutation on the forward strand.

Figure S5

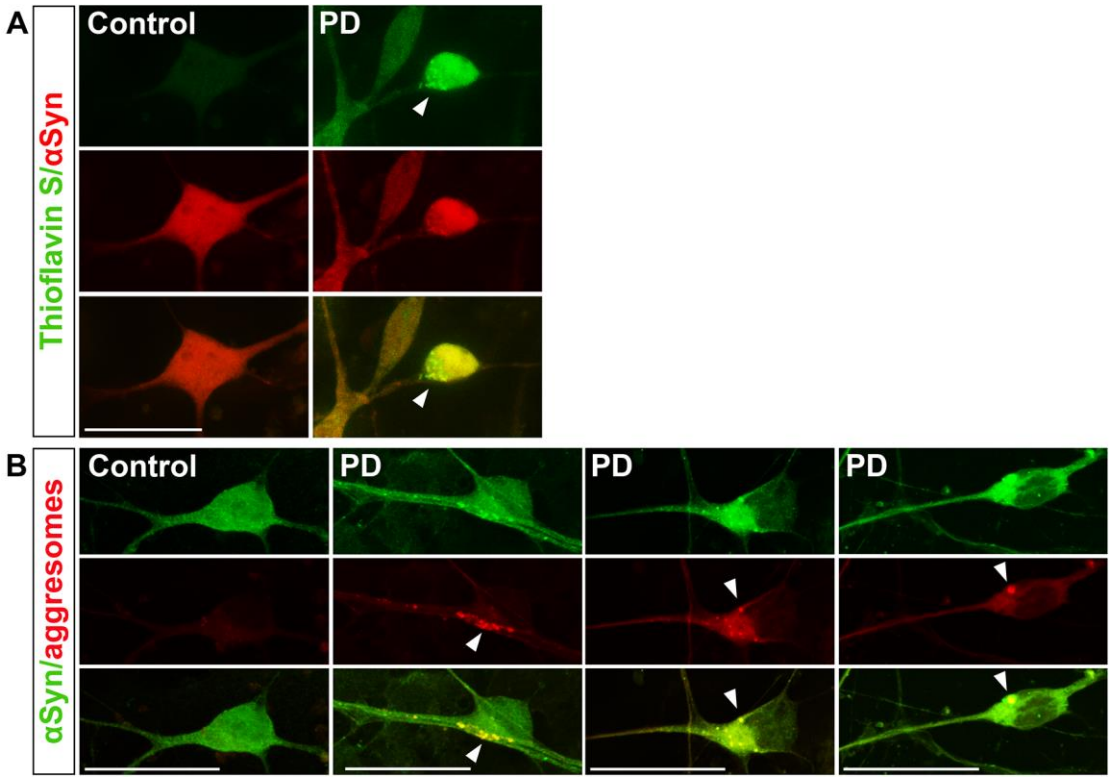

Figure S5. Detection of aggregated proteins containing αSyn, (**A**) Thioflavin S staining (green) shows protein aggregates (arrowheads) in PD iPSC-derived neurons positive for αSyn (red). Scale bar, 20 µm. (**B**) Co-staining of aggregated proteins (aggresomes; red; arrowheads) with αSyn (green). Scale bar, 20µm.

Figure S6

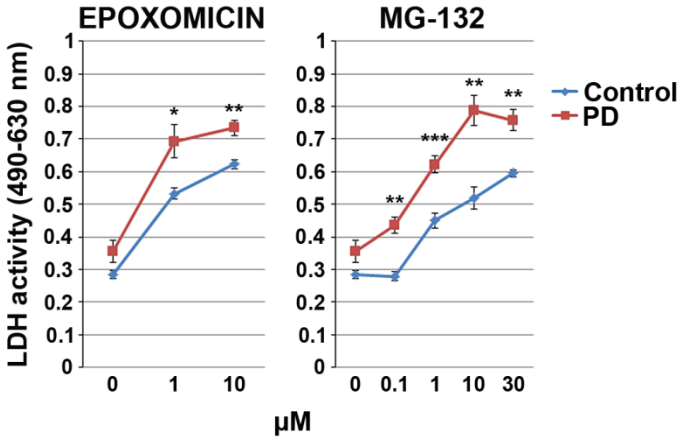

Figure S6. Dose-dependent cytotoxicity of epoxomicin and MG-132 in iPSC-derived neurons. Quantification of LDH activity (490-630 nm) in the culture supernatant, as a measure of cytotoxicity, in control and PD1 iPSC-derived neurons after treatment with epoxomicin or MG-132 for 24 h. Data represent mean ± SEM of LDH activity in supernatants derived from 3-4 wells. One experiment is shown out of two performed (Student's t-test, * $p < 0.05$, ** $p < 0.01$, *** $p< 0.001$).

Table S1A. Summary of chracterization of all iPSC lines used in the current study

Individual	Age of skin biopsy	iPSC lines	Genotype	Sex	Karyotype	Expression of pluripotency-associated markers (NANOG; TRA-1-60;SSEA4/3)	RT-PCR for pluripotency-associated markers (OCT4; NANOG; SOX2; CRIPTO)	Embryoid body formation	Teratoma formation	RNA SEQ
Control	43	C1-1	Wild-type	M	normal	+	+	+	+	+
		C1-2	Wild-type	M	normal	+	+	+	+	+
PD1	51	PD1-1	G209A SNCA mutation	M	normal	+	+	+	+	+
		PD1-2	G209A SNCA mutation	M	normal	+	+	+	+	+
PD2	38	PD2-1	G209A SNCA mutation	M	normal	+	+	+	+	-
		PD2-2	G209A SNCA mutation	M	normal	+	+	+	+	-

Table S1B. Clinical case description of patients whose cells used in the current study

Patients	Clinical Case Description
PD1	The first patient, with multiple family members affected with Parkinson's Disease, presented with a bilateral akinetic-rigid Parkinsonian syndrome at age 47. He responded well to dopaminergic treatment, but developed motor fluctuations 3 years later, at which time he also reported urge incontinence and occasional visual hallucinations on dopamine agonist therapy. When first seen at age 51, he was on an 800 mg-dose equivalent of levodopa, and was cognitively normal, with a MOCA score of 29. He was at a H&Y stage of II. Two years later however, he had developed dementia and his MOCA had dropped to 19. He experienced more frank psychosis, with persecutory delusions. He remained at a H&Y stage of II on a 700 mg dose-equivalent of levodopa.
PD2	The second patient, also with multiple family members affected with Parkinson's Disease, developed right sided Parkinsonism with tremor at age 33. He had a very good levodopa response, and continued with his occupational activities. When first seen 5 years later, he was at a H&Y stage of II, on a 700 mg dose-equivalent of levodopa. He had some mild word-finding difficulties, but was otherwise cognitively intact, with a score of 28 on the MOCA. On follow-up 2 years later he had developed autonomic symptoms (urge incontinence), postural instability, myoclonus, episodes of psychosis, and language problems of the type of expressive aphasia. MOCA had deteriorated to 12, mostly due to language issues. He was at H&Y stage of 2, on a 1000 mg dose-equivalent of levodopa. He subsequently progressed to dementia over the following 2 years.

Table S1C. Differentially expressed mRNAs between PD1 and control samples in distinct stages of differentiation

Stage of differentiation	Number of mRNA differentialy expressed (PD1 vs Control, p<0.05)
Fibroblast	1094
iPSC	342
NPC	471
Neuron	647

Table S1D. GO analysis of RNA sequencing data identified significantly affected functional categories in PD neurons

Functional Category	Number of genes ($p<0.05$)
Cell Cycle	48
Transcription/ Translation	47
Metabolism	46
Development/ Differentiation	45
Protein Vesicle/ Trafficking/ Transport	40
Signal Transduction	38
Cell Adhesion and ECM	35
Neuronal	34
Calcium Signaling	27
Immune System	18
DNA Replication/ Repair	15
Unknown	15
Other	15
Protein Modification	13
Cytoskeleton	8
Apoptosis/ Aytophagy	6

Table S1E. Analysis of RNA sequencing data using Information Hyperlinked Over Proteins" (iHOP) and PubMed-NCBI identified differentially expressed genes in PD neurons common with other Neurodegenerative Diseases

Gene Name	Ensembl ID	Parkinson's Disease	Alzheimer's Disease	Huntington's Disease	Autism	Schizophrenia	Bipolar Disorder	Reference
ADRA1A	ENSG00000120907	√				√		Tabares-Seisdedos and Rubenstein, Mol Psych, 2009
CACNA2D4	ENSG00000151062						√	Van Den Bossche et al, 2012
CBR1	ENSG00000159228	√						Tobin et al, Brain Res, 2007
CDH13	ENSG00000140945				√			Redies et al, Brain Res, 2012
CDH9	ENSG00000113100				√			Redies et al, Brain Res, 2012
CHRNA2	ENSG00000120903				√	√		Blaveri et al, 2001 (SCZ); Tabares and Rubenstein,2009 and SFARgene-Autism Database (Autism)
COMT	ENSG00000093010	√						Jimenez-Jimenez et al, 2014
CP	ENSG00000047457	√						Kristinsson et al, 2012
DES	ENSG00000175084	√						Spuler et al, 2010
DLGAP2	ENSG00000198010		√		√	√		Chien et al, 2013 (Autism); Greenwood et al, 2016 (SCZ), Chaudry et al, 2015 (AD)
EGF	ENSG00000138798	√	√					Chen-Plotkin et al, 2011
GLRA3	ENSG00000145451				√			Ramanathan et al, 2004
GRIN2D	ENSG00000105464				√	√		Tarabeux et al, 2011
GRIP2	ENSG00000144596				√			Mejias et al, 2011
HAP1	ENSG00000173805			√				Wu and Zhou, 2009
HAPLN2	ENSG00000132702					√		Fromer at al, 2014
HLA-A	ENSG00000206503				√			Torres et al, 2006; Trajkovski et al, 2015
HLADBP1	ENSG00000223865		√				√	Swaminathan et al, 2012 (AD); Choi et al, 2011 (BD)
HPCA	ENSG00000121905	√						Charlesworth et al, 2015; Nagao and Hayashi, 2009
IFITM1	ENSG00000185885					√		Hwang et al, 2013)
IL1RN	ENSG00000136689	√						Mattila et al, 2002
KCNJ10	ENSG00000177807				√			Sicca et al, 2011
KCNN3	ENSG00000143603					√		Ivkovic et al, 2006; Ritsner et al, 2002
LRRC37A2	ENSG00000238083	√						Latourelle et al, 2012; Chai et al, 2013
MSX1	ENSG00000163132	√						Deng et al, 2009
MTRNR2L1	ENSG00000256618		√					Matsuoka, 2011
NNMT	ENSG00000166741	√						Parsons et al, 2003
NPAS2	ENSG00000170485	√						Lin Q et al, 2012
NRP2	ENSG00000118257				√			Wu et al, 2007
PCNA	ENSG00000132646			√				Curtis et al, 2003
PPP2R2C	ENSG00000074211	√				√	√	Borsotto et al, 2007 (BD)Blackinton et al, 2009 (PD); Kim and Webster, 2011 (SCZ)
PTGDS	ENSG00000107317						√	Marin-Mendez et al, 2012
RPH3A	ENSG00000089169		√	√				Tan et al, 2014 (AD); Smith et al, 2007
RPP25	ENSG00000178718				√			Huang et al, 2010
SCT	ENSG00000070031				√			Krishnaswami et al, 2011
SLC6A11	ENSG00000132164				√			Griswold et al, 2012
SLITRK1	ENSG00000178235				√			Wendland et al, 2006
SLITRK2	ENSG00000185985				√	√		Piton et al, 2011
SLITRK4	ENSG00000179542				√			Purcell et al, 2014
SOX6	ENSG00000110693					√		Volk et al, 2012
SORCS1	ENSG00000108018		√					Reitz et al, 2011
SV2C	ENSG00000122012	√			√			Hills-Burns et al, 2013
SYN3	ENSG00000185666	√			√	√		Zaltieri et al, 2015 (PD); Chen et al, 2009 (SCZ)
TDO2	ENSG00000151790		√	√	√			Wu W et al, 2013 (AD); Nabi et al, 2004 (Autism); Mazarei et al, 2013
ZIC2	ENSG00000043355					√		Hatayama et al, 2011

Table S1F. 20 pre-synaptic genes differentially expressed in PD neurons

Gene Name	Ensembl ID	Fold Change	P Value
KCNA7	ENSG00000104848	-1,64667977	0,03384351
DOC2B	ENSG00000272636	-1,64164661	0,00842533
SP8	ENSG00000164651	-1,61715987	0,01915045
SCN7A	ENSG00000136546	-1,53935073	0,01602761
RPH3A	ENSG00000089169	-1,51757514	0,01524557
SLC17A9	ENSG00000101194	-1,51613563	0,01696506
SLC6A11	ENSG00000132164	-1,4857331	0,01654457
SYN3	ENSG00000185666	-1,42153279	0,02278273
TACR1	ENSG00000115353	-1,34962424	0,01198948
ASIC2	ENSG00000108684	-1,30238695	0,04590202
SV2C	ENSG00000122012	-1,24699445	0,04967023
KCNN3	ENSG00000143603	-1,23635739	0,01361471
COBL	ENSG00000106078	-1,14494704	0,03733913
SRPX2	ENSG00000102359	-1,14047787	0,03700953
ARC	ENSG00000198576	-0,9057019	0,04616589
SLC37A4	ENSG00000137700	0,986185327	0,03700146
KIFC1	ENSG00000237649	1,01964927	0,03939539
CDC20	ENSG00000117399	1,068061754	0,02811226
KIF4A	ENSG00000090889	1,583346677	0,02464734
SLC6A20	ENSG00000163817	2,924491457	0,03857758

Table S1G. 18 post-synaptic genes differentially expressed in PD neurons

Gene Name	Ensembl ID	Fold Change	P Value
CHRNA2	ENSG00000120903	-2,34358339	0,00341154
GLRA3	ENSG00000145451	-2,21931172	0,001876
GABRA4	ENSG00000109158	-1,99315369	0,01797733
SORCS1	ENSG00000108018	-1,87197851	0,03198544
GLRA1	ENSG00000145888	-1,87155259	0,00093759
DLGAP2	ENSG00000198010	-1,83467636	0,00569491
NEU4	ENSG00000204099	-1,69471714	0,00671689
GRIN2B	ENSG00000273079	-1,56718468	0,01599433
SORCS3	ENSG00000156395	-1,35218708	0,02080245
ALK	ENSG00000171094	-1,2565386	0,03563635
CHRM2	ENSG00000181072	-1,24996386	0,04626943
GRIP2	ENSG00000144596	-1,21108337	0,01536366
CHRNG	ENSG00000196811	-1,18093969	0,04770291
SLC2A3	ENSG00000059804	-1,12832065	0,01309313
GRIN2D	ENSG00000105464	-1,12461163	0,03530888
GLRA2	ENSG00000101958	-1,10023359	0,04993359
LRRC7	ENSG00000033122	-1,08766674	0,03147831
NPTX2	ENSG00000106236	-1,04458828	0,04085403

Table S1H. 5 Trans synaptic adhesion genes differentially expressed in PD neurons

Gene Name	Ensembl ID	Fold Cha	P Value
SLITRK2	ENSG00000185985	-3,8077	0,02304607
NCAM2	ENSG00000154654	-3,0383	1,407E-09
SLITRK4	ENSG00000179542	-2,0961	5,533E-05
PTPRB	ENSG00000127329	-1,5248	0,04457143
SLITRK1	ENSG00000178235	-1,3675	0,01554422

Table S1I. 13 genes of the cadherin family differentially expressed in PD neurons

Gene Name	Ensembl ID	Fold Change	P Value
PCDHA13	ENSG00000239389	-2,459152605	0,00071683
CDH13	ENSG00000140945	-2,271378714	1,8937E-05
CDH9	ENSG00000113100	-2,062740928	0,00027646
PCDH15	ENSG00000150275	-1,885564973	0,000744762
PCDHA4	ENSG00000204967	-1,590706839	0,005100768
PCDHGB2	ENSG00000253910	-1,482309748	0,025624097
PCDHA5	ENSG00000204965	-1,384175975	0,026711706
CDHR1	ENSG00000148600	-1,35554645	0,029322955
ARHGEF4	ENSG00000136002	-1,250462819	0,006892503
CDH15	ENSG00000129910	-1,006192761	0,036483845
PCDHGC5	ENSG00000240764	-0,992302675	0,037118417
PCDHAC2	ENSG00000243232	-0,938756154	0,035416413
PCDHA6	ENSG00000081842	2,26000165	0,00519631

Table S1J. 14 axon guidance-associated genes differentially expressed in PD neurons

Gene Name	Ensembl ID	Fold Change	P Value
GOLGA80	ENSG00000206127	-2,6202189	0,04361
EGF	ENSG00000138798	-2,10575423	0,00064
NTN1	ENSG00000065320	-1,51269266	0,00318
FABP7	ENSG00000164434	-1,44459068	0,00298
PLXNB3	ENSG00000198753	-1,3865818	0,00601
ARHGEF28	ENSG00000214944	-1,31402676	0,01277
SPOCK2	ENSG00000107742	-1,24751694	0,0097
NRP2	ENSG00000118257	-1,2418222	0,00884
EFNA1	ENSG00000169242	-1,23295068	0,00679
ABLIM3	ENSG00000173210	-1,11001163	0,0366
RGMA	ENSG00000182175	-1,0803274	0,02866
METRNL	ENSG00000176845	-0,94115089	0,02984
ZIC2	ENSG00000043355	1,307425909	0,00576
BTC	ENSG00000174808	2,548334324	0,00177

Table S1K. 7 genes of the WNT family differentially expressed in PD neurons

Gene Name	Ensembl ID	Fold Change	P Value
WNT3A	ENSG00000154342	4,31765781	0,0077703
WNT5A	ENSG00000114251	1,199647342	0,017924
WISP1	ENSG00000104415	-1,65497022	0,006387
RSPO1	ENSG00000169218	1,665328359	0,0017023
RSPO3	ENSG00000146374	1,646534015	0,0385925
FRZB	ENSG00000162998	0,900828372	0,0475016
DKK2	ENSG00000155011	1,230823225	0,0460819

Table S1L. 22 calcium-associated genes differentially expressed in PD neurons

Gene Name	Ensembl ID	Fold Change	P Value
CALCA	ENSG00000110680	-3,136843082	0,006491203
RCN3	ENSG00000142552	-2,421560909	2,68033E-06
RASA4B	ENSG00000170667	-1,938593736	0,000621915
HPCA	ENSG00000121905	-1,918848769	0,030704903
CCKBR	ENSG00000110148	-1,671179911	0,042988765
HMCN2	ENSG00000148357	-1,63763627	0,006203118
CABP1	ENSG00000157782	-1,633520788	0,017580271
TC2N	ENSG00000165929	-1,487836318	0,013644413
RASA4	ENSG00000105808	-1,450265236	0,010465597
FAM69C	ENSG00000187773	-1,400876449	0,005407353
CACNA2D4	ENSG00000151062	-1,333439528	0,016408848
JSRP1	ENSG00000167476	-1,298681765	0,039962141
SPOCK2	ENSG00000107742	-1,247516938	0,009699784
S100A6	ENSG00000197956	-1,19402578	0,020194304
ADRA1A	ENSG00000120907	-1,111123759	0,044719722
CACNA1D	ENSG00000157388	-1,101306844	0,031855521
JPH2	ENSG00000149596	-1,072292853	0,043904426
PITPNM2	ENSG00000090975	-1,008409372	0,042073728
SMOC1	ENSG00000198732	0,935445851	0,047195293
EFHB	ENSG00000163576	1,19038159	0,041089127
TMBIM4	ENSG00000155957	1,9554334	0,011660053
CCBE1	ENSG00000183287	1,98354615	0,001627327

Table S2A. List of primer sequences used in the current study

Gene Name	Application	Forward	Reverse
ABLIM3	qPCR	ACTACCATGCCCAGTTTGG	GTACATTTCCTCTCCTTCGGTG
CDH13	qPCR	CAGAGACAGCCTTTCCCAAG	GAGACGCTCCCTGTGTTCTC
CDH15	qPCR	CTCTATCGACAAGTTCACAGGG	CCACAACTACAATCTCCAGGTC
CRIPTO	RT-PCR	TACCTGGCCTTCAGAGATGACA	CCAGCATTTACACAGGGAACAC
DLGAP2	qPCR	AAAGTCGGCAATCCTACCAG	GGGAGTTGTAGTTCGCAGC
DOC2B	qPCR	ACAGATGAAGACATGATCCGC	TCTTGGTGTGGTTGGGTTTC
EFNA1	qPCR	TTCACACCTTTCACCCTGG	ACAGTCACCTTCAACCTCAAG
FABP7	qPCR	AGGACTCTCAGCACATTCAAG	CTTTGCCATCCCATTTCTGTATG
FOXA2	qPCR	CCATGCACTCGGCTTCCAG	TGTTGCTCACGGAGGAGTAG
GAD67	qPCR	GCCAGACAAGCAGTATGATGT	CCAGTTCCAGGCATTTGTTGAT
GAPDH	qPCR	CCTCTGACTTCAACAGCGACAC	AGCCAAATTCGTTGTCATACCAG
GAPDH	RT-PCR	GATGACATCAAGAAGGTGGTGA	GTCTACATGGCAACTGTGAGGA
GRIN2D	qPCR	GTACGTGGATACTGTGTCTGG	TGTGCATGTCGGGATAGTTG
GRIP2	qPCR	CTACACCCTTGGAGATGCAC	TCTGAGACGCTGAAACCAAAG
HPCA	qPCR	CCTTCAGCATGTATGACCTGG	TTTCTCAGTCCTCTTTTCCGG
MAP2	qPCR	GAGAATGGGATCAACGGAGA	CTGCTACAGCCTCAGCAGTG
NANOG	RT-PCR	AGTCCCAAAGGCAAACAACCCACTTC	TGCTGGAGGCTGAGGTATTTCTGTCTC
NESTIN	qPCR	TCCAGGAACGGAAAATCAAG	GCCTCCTCATCCCCTACTTC
NTN1	qPCR	CAAGAGCGGAGGTGTCTG	ACAGGGTGGCAATCACAG
NURR1	qPCR	TCGACATTTCTGCCTTCTCCTG	GGTTCCTTGAGCCCGTGTCT
OCT4	RT-PCR	ATGCACAACGAGAGGATTTTGA	CTTTGTGTTCCCAATTCCTTCC
PAX6	qPCR	TGTCCAACGGATGTGTGAGT	TTTCCCAAGCAAAGATGGAC
PITX3	qPCR	GAGCTAGAGGCGACCTTCC	CCGGTTCTTGAACCACACCC
RCN3	qPCR	ACATACGGGACTCGGTGAG	TTTTGTAGGTCTCTGCATCCTC
RPH3A	qPCR	CAGAGGAAGCAGGAAGAGC	TCATGTTTTCTAGGCGGTCC
SLITRK1	qPCR	ACTCTTCCTACTGGCACAATG	GATGTATCGCCTTCCCTCTG
SLITRK2	qPCR	CTCGATGGACACAGGAAGATC	GCAAAGCTCAATTCCCGG
SLITRK4	qPCR	GTCCTTGAGGAGCAAACAGC	CTGCCTCCATGCCTATTGAT
SNCA	qPCR	GGAGTGGCCATTCGACGAC	CCTGCTGCTTCTGCCACAC
SNCA	PCR	GCTAATCAGCAATTTAAGGCTAG	GATATGTTCTTAGATGCTCAG
SOX2	RT-PCR	TTACCTCTTCCTCCCACTCCAG	GGGTTTTCTCCATGCTGTTTCT
SV2C	qPCR	GTGTTTGTCATCGTCTGTGC	GGCTCTCATGTTGGTGTCAT
SYN3	qPCR	CTACTCCGTCTACAACTTCTGC	GCTGTGACCATTGGCTTATG
TH	qPCR	TGTCTGAGGAGCCTGAGATTCG	GCTTGTCCTTGGCGTCACTG
VGLUT1	qPCR	CGACGACAGCCTTTTGTGGT	GCCGTAGACGTAGAAAACAGAG

Table S2B. Antibodies used in the current study

Name	Host	Dilution	Vendor	Catalog#
Anti-α-fetoprotein (AFP)	Mouse	1/200	Merck-Millipore	2004189
Anti-cleaved caspase-3 (cCASP3)	Rabbit	1/400	Cell Signalling	9661S
Anti-GABA	Rabbit	1/10000	Sigma-Aldrich	A2052
Anti-GAPDH	Mouse	1/1000	Santa Cruz Biotechnology	sc-365062
Anti-MAP2	Mouse	1/200	Merck-Millipore	MAB3418
Anti-NANOG	Goat	1/100	R&D Systems	AF1997
Anti-NESTIN	Rabbit	1/200	Merck-Millipore	ABD69
Anti-PAX6	Mouse	1/100	DSHB	AB 528427
anti-PSD95	Mouse	1/100	Merck-Millipore	MABN68
Anti-smooth muscle actin (SMA)	Mouse	1/200	Merck-Millipore	CBL171
Anti-SOX2	Rabbit	1/1000	Abcam	ab59776
Anti-SSEA3	Mouse	1/100	DSHB	MC-631
Anti-SSEA4	Mouse	1/100	DSHB	MC-813-70
Anti-Synapsin 1 (SYN1)	Rabit	1/200	Cell Signalling	D12G5
Anti-α-Synuclein (αSyn)	Mouse	1/500	BD Biosciences	610787
Anti-phosphorylated α-Synuclein (Ser129)	Mouse	1/10000	WAKO	015-25191
Anti-phosphorylated α-Synuclein (Ser129)	Rabbit	1/1000	Abcam	ab51253
Anti-TAU	Mouse	1/500	Thermo Fisher Scientific	MN1000
Anti-TH	Rabbit	1/500	Merck-Millipore	AB152
Anti-TH	Mouse	1/200	Merck-Millipore	MAB318
Anti-TRA-1-60	Mouse	1/200	Merck-Millipore	MAB4360
Anti-TUJ1	Rabbit	1/1000	Cell Signalling	5568
Anti-VGLUT1	Mouse	1/1000	Merck-Millipore	MAB5502